

# Improving SMOTE via Fusing Conditional VAE for Data-adaptive Noise Filtering

Sungchul Hong<sup>1</sup>, Seunghwan An<sup>2</sup>, Jong-June Jeon<sup>1\*</sup>

<sup>1</sup>Department of Statistics, University of Seoul, 163 Seoulsiripdaero, Seoul, 02504, South Korea.

<sup>2</sup>Department of Statistical Data Science, University of Seoul, 163 Seoulsiripdaero, Seoul, 02504, South Korea.

\*Corresponding author(s). E-mail(s): [jj.jeon@uos.ac.kr](mailto:jj.jeon@uos.ac.kr);  
Contributing authors: [shong@uos.ac.kr](mailto:shong@uos.ac.kr); [dkstmdghks79@uos.ac.kr](mailto:dkstmdghks79@uos.ac.kr);

## Abstract

Recent advances in a generative neural network model extend the development of data augmentation methods. However, the augmentation methods based on the modern generative models fail to achieve notable performance for class imbalance data compared to the conventional model, the SMOTE. We investigate the problem of the generative model for imbalanced classification and introduce a framework to enhance the SMOTE algorithm using Variational Autoencoders (VAE). Our approach systematically quantifies the density of data points in a low-dimensional latent space using the VAE, simultaneously incorporating information on class labels and classification difficulty. Then, the data points potentially degrading the augmentation are systematically excluded, and the neighboring observations are directly augmented on the data space. Empirical studies on several imbalanced datasets represent that this simple process innovatively improves the conventional SMOTE algorithm over the deep learning models. Consequently, we conclude that the selection of minority data and the interpolation in the data space are beneficial for imbalanced classification problems with a relatively small number of data points.

**Keywords:** SMOTE, Imbalanced Classification, Variational Autoencoder, Oversampling

# 1 Introduction

Class imbalance problem is a common challenge in constructing a classification model [1]. The empirical risk minimization method tends to underrepresent the features of observations belonging to the minor class, thereby inducing bias in the learning model and detrimentally affecting its performance. Oversampling the minor class is a popular technique to mitigate the class imbalance problem. Oversampling involves generating synthetic instances for the minor class and resampling to balance the class distribution. Under lack of data, it is often regarded as an essential preprocessing step in various domains, including medical diagnosis, defect detection, and chemical classification [2–4].

Synthetic Minority Oversampling Technique (SMOTE) [5] generates new minor class samples by interpolating between existing minor class samples and their nearest minority neighbors. Due to its simplicity and effectiveness, SMOTE has become a standard approach in the field of imbalanced classification [6]. Building on the success of SMOTE, several extensions [7] have been proposed to further enhance classification performance, especially under scenarios involving specific data structures or mislabeling. These extensions include Borderline-SMOTE [8], and ADASYN [9]. These methods aim to address the limitations of SMOTE and are discussed in detail in Section 2.

The advent of effective dimensionality reduction and generative model learning for high-dimensional data has facilitated easier generation of data belonging to the minor class, leading to a significant expansion beyond conventional oversampling methods. Some of these techniques employ neural networks to enhance the oversampling performance [10–12]. Additionally, deep learning approaches efficiently augment unstructured datasets such as image and text [13, 14]. These techniques leverage the power of deep neural networks to generate synthetic samples that are more representative of the minor class, improving the performance of models on image and text classification tasks.

Accordingly, deep generative models (DGMs), such as Variational AutoEncoders (VAEs) [15] and Generative Adversarial Networks (GANs) [16], are adapted to oversampling. Specifically, the VAE maps high-dimensional data into a lower-dimensional latent space by feature extraction. These approaches effectively encode the underlying characteristics of imbalanced datasets by utilizing the latent space [17, 18]. However, [19] claims that oversampling based on DGMs does not yield substantial improvements over SMOTE, particularly in tabular datasets. They conjecture the limitation of DGM-based oversampling techniques is attributed to the inaccurate estimation of the density function in an imbalanced dataset. They raise doubts about whether learning the distribution of the major class would significantly contribute to identifying the distribution of the minor class. Motivated by the empirical evidence of [19], we investigate the pattern of the augmented samples of DGMs with the *Escherichia coli* dataset [20] to understand why the DGMs often fail to improve the prediction model.

First, we visualize the latent space obtained by typical DGMs, the conditional VAE, and the Autoencoder (AE)-based DDHS [21]. Figure 1 displays observations on the trained latent space. The observations are labeled as easy-major, hard-major, easy-minor, and hard-minor classes according to their classification difficulty and class

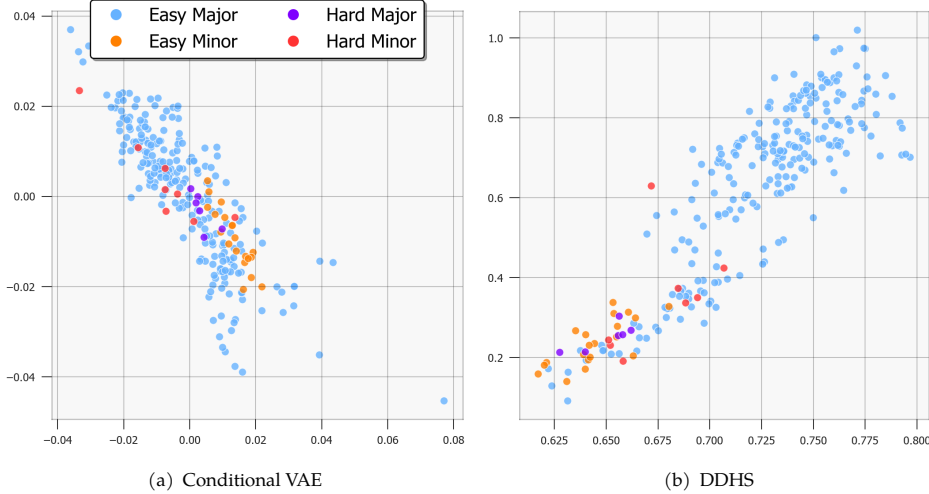


**Fig. 1** Visualization of latent space of Conditional VAE and DDHS.

majority. The classification difficulty is quantified as a local misclassification error obtained by the K-nearest neighbor algorithm. We can see that the minority samples are overlapped with the major samples in the latent space. In addition, Figure 1 shows that the embedding latent space is unlikely to contain the information of the classification difficulty. Thus, SMOTE or neighborhood sampling methods often learn a distribution of major samples as that of minority samples.

Second, the estimation of distribution for minority samples is vulnerable to noise or outliers. In particular, when the minor class exhibits within-class imbalance, naive distributional learning can mislead to oversampling, pursuing the generation of so-called high-quality synthetic instances. This challenging problem is called the small-disjunct problem [1, 22]. In the conventional kernel density estimation studies, the adaptive bandwidth selection method is recommended for more accurate distributional learning [23]. In both Figure 1 (a) and (b), we can see a hard-minority sample distant from the center of the minority samples. Interpolation on the latent space between this observation and other neighborhoods produces synthetic samples far from the minor group.

The main idea underlying our oversampling method revolves around contrasting the pattern of interest. The proposed oversampling consists of three steps. The algorithm explores the latent space in which the majority and classification difficulty are embedded. To disentangle the mode of each class in the latent space, we employ the VAE [24] capable of aligning an encoded feature of a specific class at a pre-determined prior mode. Next, with the trained latent structure, we exclude the samples that do not contain neighboring information belonging to the same class [25]. A density-based filtering removes isolated observations, regarded as outliers in the latent space. Finally, we employ SMOTE directly to the filtered observations, not latent variables.

The advantages of our method are listed as follows:

1. The proposed method involves disentangling the latent space based on various features under consideration for data augmentation with a state-of-the-art VAE. Thus, we can gain insights into the distinguished nature of labels, effectively separating latent variables based on a predefined prior distribution.
2. We enhance the existing methods to identify and remove a noise sample by considering proximity in the separated latent space. Through filtering, we can prevent a noise sample from being involved in SMOTE so that we partly solve the low-quality problem, such as unrealistic synthetic samples and ignoring variable dependencies, by DGMs [25].
3. We demonstrate the efficiency and superiority of our proposed method. Numerical studies show that our simple disentangling and filtering step can effectively improve the classification performance of the Area Under the Precision-Recall Curve (AUPRC) and the Area Under the Curve (AUC).

The remainder of this paper is organized as follows: Section 2 introduces the existing oversampling method containing classical and deep learning-based approaches. Section 3 explains the proposed algorithm by dividing it into two parts: customizing latent space and oversampling with filtering. Section 4 shows the numerical results using synthetic and real datasets with various visualizations. Concluding remarks and limitations of this paper follow in Section 5.

## 2 Related Work

### 2.1 Overview

An ideal oversampling method is to sample from the true distribution of the minor class. Thus, estimating a target distribution is a natural and intuitive approach to developing an oversampling method. However, this can be particularly challenging in high-dimensional settings under a lack of data. Despite the notable advances of a generative model driven by deep learning, developing a novel oversampling method is discouraging. It is important to note that deep learning-based approaches still face challenges in accurately estimating the density of the minor class, and this limitation can impede their effectiveness in oversampling tasks. We will investigate this issue in more detail in Section 4. Thus, it is common for researchers to define the specifics of their task and then apply a suitable oversampling method, as demonstrated in survey works [1, 22]. For binary classification problems, it is generally assumed that generated synthetic samples can aid in finding the optimal decision boundary, leading to oversampling in the vicinity of the minority samples.

SMOTE [5] is a straightforward oversampling method that linearly interpolates between two neighboring minority samples. This method samples from restricted low dimensional space (a subset of low dimensional convex hull) and achieves superior performance [26]. However, SMOTE is still vulnerable to noise and is often unable to effectively address the issue of small disjuncts, which refer to small-sized clusters within the minor class and incur false negatives.

The proposed oversampling method is an extension of existing research enhancing the performance of SMOTE. The novelty distinguished from the prior studies

lies in filtering minority samples on a low-dimensional latent space, reflecting the pre-defined characteristics of data. In particular, our proposed method focuses on selecting appropriate minority samples for oversampling and mitigating the issues associated with small disjuncts, ultimately improving the performance of imbalanced classification. In the following subsection, we introduce an extended study of SMOTE, presenting an oversampling method that utilizes deep learning as a comparative model.

## 2.2 Literature review

This section provides a comprehensive review of oversampling literature, specifically focusing on data-level oversampling approaches, including SMOTE-based, AE-based, and VAE-based methods.

**SMOTE-based methods.** SMOTE [5] generates new synthetic samples by linearly interpolating between minority samples and their K-nearest neighbors among the minority samples. SMOTE is a simple and powerful augmentation method, but its theoretical properties are rarely known. Elreedy et al. [27] analyzes the distribution of the augmented samples by SMOTE. Because SMOTE does not perform well on highly noisy datasets, [8] proposes Borderline-SMOTE incorporating a selection step to identify necessary minority samples known as “borderline samples”. These samples are chosen based on neighborhood information, specifically the ratio of major samples to the total number of neighbors. Another approach to address class imbalance is ADASYN [9]. A data-adaptive oversampling method assigns weights to minority samples based on their neighborhood information. This adaptive weighting scheme emphasizes the minority samples that are more challenging to classify correctly. Another approach to noise is SMOTE-ENN [28], which synthesizes minority samples by SMOTE and filters noise out by the edited nearest neighborhood (ENN). However, these approaches primarily rely on neighborhood information and do not consider the characteristics on feature levels. To address imbalance within the class, KMSMOTE is proposed by [29]. KMSMOTE constructs clusters regardless of class by K-means clustering and then calculates the ratios of the minority samples in clusters. After clustering, KMSMOTE identifies clusters whose ratio of minority samples is too low and filters them out. However, this method has some limitations in that hyperparameters (e.g., the number of clusters) tuning is required, and its performance is sensitive to them.

**AE-based methods.** The neighborhood information used in SMOTE-based methods is typically induced by Euclidean distance defined on data space. The Euclidean distance is often an inadequate metric representing the proximity between data points, especially in high-dimensional cases. To address this issue, various methods leverage autoencoder architectures to learn lower-dimensional representations of the data. These lower-dimensional representations retain essential information, enabling the reconstruction of the original data. Many oversampling methods propose various architectures of AEs and loss functions. Dablain et al. [11] proposes the AE-based oversampling algorithm, DeepSMOTE, which employs SMOTE to synthesize the latent variables with the minor label. DeepSMOTE uses a loss function based on U-statistics to minimize within-class variances, aiming to create a desirable

latent space. Other methods, such as DFBS [10] and DDHS [21], leverage the center loss [30] to learn discriminative latent features. They also propose novel methods for generating high-quality and various features focusing on a minor class.

**VAE-based methods.** Variational AutoEncoders (VAEs) have derived practical applications in generating high-dimensional datasets, and the theoretical foundations of VAEs have led to extensions and adaptations in various domains. For instance, Fajardo et al. [18] employ Conditional VAEs (CVAEs) to synthesize minority samples, while Dai et al. [17] extend VAEs for discriminative feature learning within a contrastive learning framework. In the context of multi-class classification, Solomon et al. [31] propose a novel VAE framework designed to preserve the data structure based on their class labels. However, similar to AE-based methods, these VAE-based approaches fail to separate the latent space. Additionally, they may suffer from generating poor-quality synthetic samples due to the inherent trade-off between KL-divergence and reconstruction errors.

In contrast to the above literature, our approach introduces a two-step filtering algorithm that can be combined with various oversampling techniques. The filtering algorithm considers not only the local information of the samples themselves but also identifies anomalies within each group in the latent space. This sophisticated filtering improves classic oversampling algorithms, making them more effective in low- and high-dimensional datasets when compared to deep learning approaches.

### 3 Proposed Method

This section introduces SMOTE-CLS (SMOTE with Customizing Latent Space), a novel oversampling technique that combines SMOTE with a customized latent space generated by a conditional VAE. Section 3.1 elaborates on the approach used to handle the sample difficulties and manipulate the latent space. Following that, in Section 3.2, we will describe our oversampling methodology, which relies on utilizing the trained latent space.

#### 3.1 Customizing Latent Space with VAE

First, we introduce the notations used throughout this paper. Let  $\mathbf{x}_i \in \mathcal{X}$  and  $y_i \in \mathcal{Y} = \{M, m\}$  for  $i = 1, \dots, n$  be the predictors and labels where  $M$  and  $m$  are labels associated with the major and minor classes, respectively. Inspired by [8] and [32] identifying a sample difficulty, we categorize the samples into two distinct groups again: “easy sample” and “hard sample” based on their local information that easy samples are more prototypical with their neighborhoods while hard samples are less prototypical.

To obtain the information straightforwardly, we employ the K-nearest neighbors (KNN) classifier, denoted as  $f_K : \mathcal{X} \mapsto \mathcal{Y}$ , and define the relabeling map  $g : \mathcal{X} \times \mathcal{Y} \mapsto$

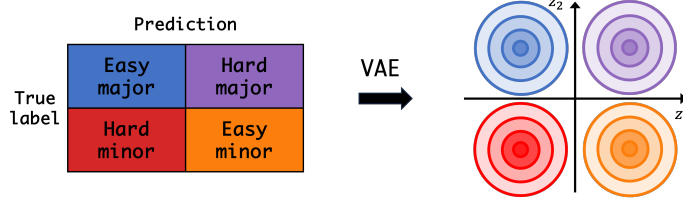


**Fig. 2** An example of constructing prior distribution. Classification confusion matrix generated by the KNN classifier (left), the prior distribution,  $p(\mathbf{z}|y)$  (right). We set the expectation of prior distribution as follows:  $\mu_M = (-1, 1)$ ,  $\mu_m = (1, -1)$ ,  $\mu_{M^*} = (1, 1)$ , and  $\mu_{m^*} = (-1, -1)$ .

$\mathcal{Y}^* = \{M^*, m^*, M, m\}$  in (1).

$$g(\mathbf{x}, y; f_K) = \begin{cases} M^*, & \text{if } y = M \text{ and } f_K(\mathbf{x}) \neq y \\ m^*, & \text{if } y = m \text{ and } f_K(\mathbf{x}) \neq y \\ M, & \text{if } y = M \text{ and } f_K(\mathbf{x}) = y \\ m, & \text{if } y = m \text{ and } f_K(\mathbf{x}) = y \end{cases}. \quad (1)$$

Let a pseudo label indicating both the class and the classification difficulty by the KNN be

$$\tilde{y}_i = g(\mathbf{x}_i, y_i; f_K)$$

for  $i = 1, \dots, n$ . Consequently, the labels of data,  $\tilde{y}_i$ s, are refined by hard-major  $M^*$ , hard-minor  $m^*$ , easy-major  $M$ , and easy-minor group  $m$ , respectively. Accordingly let  $D_{M^*} = \{i | \tilde{y}_i = M^*\}$ ,  $D_{m^*} = \{i | \tilde{y}_i = m^*\}$ ,  $D_M = \{i | \tilde{y}_i = M\}$ , and  $D_m = \{i | \tilde{y}_i = m\}$ .

Building upon the previous relabelling, we segment the latent space with major and minor labels and their classification difficulty. We assume that easy and hard samples possess distinct characteristics preserved in the latent space within the major and minor classes. Denote the latent space by  $\mathcal{Z}$ . For each label  $c \in \mathcal{Y}^*$ , we assume  $\mathbf{z} | \tilde{y} = c \sim \mathcal{N}(\mu_c, \text{diag}(s_c^2))$ . The marginalized prior distribution  $p(\mathbf{z})$  is a Gaussian Mixture Model (GMM) as follows:

$$p(\mathbf{z}) = \sum_{c \in \mathcal{Y}^*} p(\tilde{y} = c) \cdot \mathcal{N}(\mu_c, \text{diag}(s_c^2)).$$

The conditional VAE with the priors allows us to manipulate the latent space based on the classification difficulty defined in (1). Figure 2 presents an example of latent space by sample difficulty. In Section 4.2, we investigate the effect of structural constraint on the prior distribution. In addition, this conditional VAE is different from the conventional one, such as CVAE [33], because it utilizes the pseudo labels for a specific disentanglement of the latent space.

We employ an encoder  $q_{\phi, \eta}(\mathbf{z} | \mathbf{x})$  to approximate  $p(\mathbf{z} | \mathbf{x})$ .

$$q_{\phi, \eta}(\mathbf{z} | \mathbf{x}) = \sum_{c \in \mathcal{Y}^*} f_{\eta}(\tilde{y} = c | \mathbf{x}) \cdot q_{\phi}(\mathbf{z} | \tilde{y} = c, \mathbf{x}), \quad (2)$$

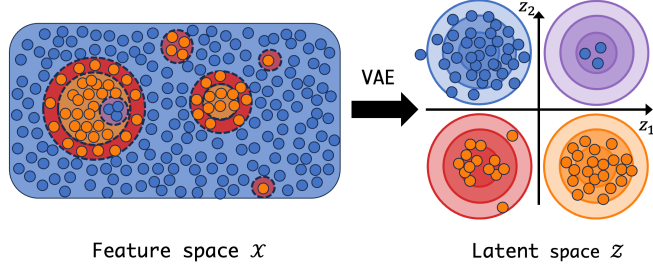


**Fig. 3** An example of the process of customizing latent space based on the classification difficulty from original feature space  $\mathcal{X}$  (left) to latent space  $\mathcal{Z}$  (right). Blue and orange points denote major and minor samples. The classification difficulty defined by (1) corresponding to the colors as follows: **blue**: easy-major, **orange**: easy-minor, **purple**: hard-major, **red**: hard-minor.

where  $f_\eta$  is a classifier with a parameter  $\eta$ . Each component of Gaussian mixture (2) is defined as  $q_\phi(\mathbf{z}|\tilde{y} = c, \mathbf{x}) = \mathcal{N}(\mathbf{z}|\boldsymbol{\mu}_c(\mathbf{x}; \phi), \text{diag}(\sigma_c^2(\mathbf{x}; \phi)))$ . Then the evidence lower bound (ELBO) of  $p(\mathbf{x}, \tilde{y})$  is derived by

$$\begin{aligned}
& \log p(\mathbf{x}, \tilde{y}; \theta, \sigma) \\
&= \log p(\mathbf{x}; \theta, \sigma) + \log p(\tilde{y}|\mathbf{x}; \theta, \sigma) \\
&\geq \mathbb{E}_q[\log p(\mathbf{x}|\mathbf{z}; \theta, \sigma)] - D_{KL}(q_{\eta, \phi}(\mathbf{z}|\mathbf{x})\|p(\mathbf{z})) + \log p(\tilde{y}|\mathbf{x}; \theta, \sigma) \\
&\simeq \mathbb{E}_q[\log p(\mathbf{x}|\mathbf{z}; \theta, \sigma)] - D_{KL}(q_{\eta, \phi}(\mathbf{z}|\mathbf{x})\|p(\mathbf{z})) + \log f_\eta(\tilde{y}|\mathbf{x}),
\end{aligned}$$

where the decoder  $p(\mathbf{x}|\mathbf{z}; \theta, \sigma)$  is assumed as Gaussian distribution,  $\mathcal{N}(D(\mathbf{z}; \theta), \text{diag}(\sigma^2))$ , and  $D(\cdot; \theta)$  is a neural network with parameter  $\theta$ . Because, however,  $D_{KL}(q(\mathbf{z}|\mathbf{x}; \eta, \phi)\|p(\mathbf{z}))$  in the ELBO does not possess a closed-form solution, we use its upper bound,  $D_{KL}^U(q_{\eta, \phi}(\mathbf{z}|\mathbf{x})\|p(\mathbf{z}))$  instead.

$$\begin{aligned}
& D_{KL}^U(q_{\eta, \phi}(\mathbf{z}|\mathbf{x})\|p(\mathbf{z})) \\
&= \sum_{c=1}^C f_\eta(\tilde{y} = c|\mathbf{x}) D_{KL}(q_{\eta, \phi}(\mathbf{z}|\mathbf{x}, \tilde{y} = c)\|p(\mathbf{z}|\tilde{y} = c)) + D_{KL}(f_\eta(\tilde{y}|\mathbf{x})\|p(\tilde{y}))
\end{aligned}$$

Therefore, our objective function of VAE is given by

$$L(\theta, \eta, \phi) = \mathbb{E}_q[\log p(\mathbf{x}|\mathbf{z}; \theta, \sigma)] - D_{KL}^U(q_{\eta, \phi}(\mathbf{z}|\mathbf{x})\|p(\mathbf{z})) + \log f_\eta(\tilde{y}|\mathbf{x}). \quad (3)$$

Details of deriving (3) can be found in [24].

In our approach, we train the VAE to maximize the objective function (3). Following the semi-supervised learning perspective, the classifier  $f_\eta$  in (3) is simultaneously trained with the VAE, and the latent space is disentangled by the trained classifier predicting  $\tilde{y}$ . Since  $\tilde{y}$  contains the information on classification difficulties and labels, the trained latent space can be constructed more elaborately to reflect features of an isolated observation. Furthermore, this study investigates the impact of  $f_\eta$  on modeling



the latent space (see Appendix A1). We use tree-based classifiers to enhance performance, particularly in tabular datasets, such as a random forest [34] or XGBoost [35]. This approach improves performance and reduces the computational cost of training neural networks. Figure 3 provides a visual summary of the process discussed in Section 3.1.

### 3.2 Oversampling with Filtering

To generate high-quality minority samples, selecting high-quality candidates for oversampling is essential. The definition of ‘high quality’ often involves utilizing distance or density measures to distinguish between instances, as demonstrated in previous studies [10, 21, 36]. However, these existing approaches can be overly conservative, focusing solely on easy samples or sensitive to outliers, rendering them vulnerable to noise. For instance, Liu et al. [10] proposes a selection method as a high-quality candidate for oversampling with a distance between a sample and each class centroid. This approach is susceptible to noise samples because the centroid is sensitive to outliers (see Section 4.1), and the centroid inaccurately represents the locational characteristic of a mixture distribution.

Liu and Chang [21] defines high-quality minority samples as the minor class observations with a high density. As a result, only easy samples, in our definition labeled (1) by  $\tilde{y} = m$ , are selected, and hard samples tend to be excluded in the sampled candidates (see Section 4.1). To avoid this problem and simultaneously identify noise samples, we modulate the filtering process with a density function for each of two classes,  $m^*$  and  $m$  in (1). For example, the latent variables labeled by  $m^*$  form clusters by a predefined prior distribution  $p(\mathbf{z}|\tilde{y} = m^*)$  (See Figure 2). Consequently, we identify noise samples as outliers from each cluster, and their noise level is assessed based on each density.

Despite a specification of the prior distribution in VAE, the posterior distribution  $q_{\phi,\eta}(\mathbf{z}|\mathbf{x})$  may not perfectly align with the predefined priors. As a solution, previous works such as [37] and [38] employed a two-stage approach, utilizing GMM on the latent space. Additional estimation of the posterior enables a more accurate diagnosis of latent variables.

Building on the motivation from prior works, we incorporate the Kernel Density Estimation (KDE) on the latent space with the filtering process. We estimate the density of hard and easy-minority samples by KDE to consider the distributional property of each group. Let latent variables from the easy-minority samples be

$$\mathbf{z}_i = \boldsymbol{\mu}_c(\mathbf{x}_i; \phi),$$

where  $c = \operatorname{argmax}_k f_\eta(\tilde{y} = k|\mathbf{x}_i)$  for  $i \in D_m$ . Recall that  $\boldsymbol{\mu}_c(\mathbf{x}_i; \phi)$  and  $f_\eta(\tilde{y} = k|\mathbf{x}_i)$  are the mean vector and classifier in (2). Let  $\hat{f}_m(\mathbf{z})$  be the estimated density of the latent variables of easy-minority samples by KDE. The bandwidth of KDE is determined using a conventional bandwidth selection method, Scott’s rule [39] to ensure more accurate density estimation, particularly when dealing with varying numbers of samples [40]. Similarly, we estimate the densities of the latent variables from the hard-minority samples,  $\hat{f}_m^*(\mathbf{z})$  by the KDE. Using threshold  $\tau$  to filter out noise,

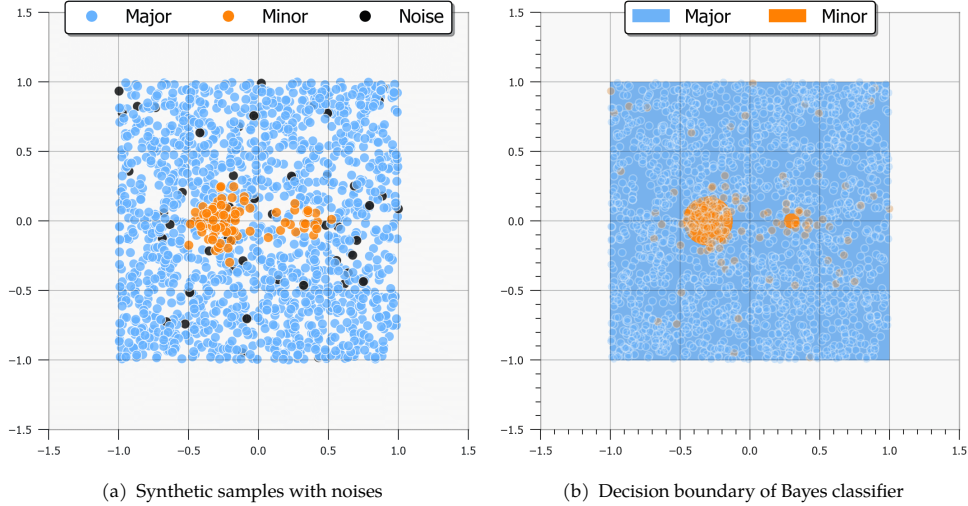


**Fig. 4** Visualization of the synthetic dataset. The sky blue, orange, and black points are major, minor, and noise samples.

we select minor latent variables whose densities are larger than  $\tau_s$  in each group. This difficulty-adaptive filtering scheme ensures the robustness of our algorithm to the parameters of predefined priors. Please refer to Section 4.2 and Appendix A2 for further exploration and details. In the implementation, we set  $\tau_1$  and  $\tau_2$  below which the observations with density  $\hat{f}_m(\mathbf{z})$  are excluded in the easy and hard-minor classes. Visualizations of the latent space can assist in selecting the threshold values  $\tau_s$  empirically (see Appendix A3).

Once the filtering process is completed, let a subset of the minority samples with selected features denoted as  $\tilde{\mathbf{X}}_m$ :

$$\tilde{\mathbf{X}}_m = \{\mathbf{x}_i \mid \hat{f}_m(\mathbf{z}_i) > \tau_1, i \in D_m\} \cup \{\mathbf{x}_i \mid \hat{f}_{m^*}(\mathbf{z}_i) > \tau_2, i \in D_m^*\}.$$

Finally, we apply the conventional SMOTE on  $\tilde{\mathbf{X}}_m$  to generate synthetic minority samples. The entire process of our method is summarized in Algorithm 1.

## 4 Numerical Studies

In this section, we conduct numerical studies using synthetic and 12 real datasets. The simulation study with the synthetic dataset aims to investigate how our proposed method identifies noise samples within the minor group and effectively filters them out. We compare our method with other competitive oversampling methods in real data analysis. Our experiments are implemented with PyTorch on a Mac equipped with an Apple M2 Max processor and 32GB of RAM.

---

**Algorithm 1: SMOTE-CLS Algorithm**

---

**Input** : Model parameters:  $\theta, \phi$ ; Prior distribution  $p(\mathbf{z})$ ; Learning rate:  $\alpha$ ;  
KNN classifier:  $f_K$ ; Classifier:  $f_\eta$ ; KL-divergence weight:  $\beta$ ;  
Thresholds:  $\tau_1, \tau_2$ ; oversampling ratio:  $\rho$ .

**Output:** Augmented minor set.

- 1 **Identifying Sample's Difficulty**
  - for  $i = 1, \dots, n$  do
  - 2 |  $\tilde{y}_i = g(\mathbf{x}_i, y_i; f_K)$
  - 3 end
  - 4 Let  $D_m^* = \{i | \tilde{y}_i = m^*\}$ ,  $D_m = \{i | \tilde{y}_i = m\}$ ,  $D_M^* = \{i | \tilde{y}_i = M^*\}$ , and  $D_M = \{i | \tilde{y}_i = M\}$ .
  - Train the Classifier**  $f_\eta$ .
  - Train the VAE:** for  $e \leftarrow epochs$  do
  - 5 | Draw a random subset  $\mathcal{B} \subset \{1, \dots, n\}$ 
    - for  $j \in \mathcal{B}$  do
    - 6 |  $\mathbf{z}_j \sim q_{\eta, \phi}(\mathbf{z} | \mathbf{x}_j)$   
 $\hat{\mathbf{x}}_j \leftarrow p(\mathbf{x} | \mathbf{z}_j; \theta, \sigma)$
    - 7 end
    - 8  $L = \sum_{j \in \mathcal{B}} |\mathbf{x}_j - \hat{\mathbf{x}}_j| + \beta \cdot D_{KL}^U(q_{\eta, \phi}(\mathbf{z} | \mathbf{x}_j) || p(\mathbf{z}))$   
 $\theta \leftarrow \theta - \alpha \frac{\partial L}{\partial \theta}$   
 $\phi \leftarrow \phi - \alpha \frac{\partial L}{\partial \phi}$
    - 9 end
  - 10 **Group Adaptive Filtering:**  
Define the latent variable of  $\mathbf{x}, \mathbf{z}$  as follows:  
 $\mathbf{z} = \boldsymbol{\mu}_c(\mathbf{x}; \eta)$  where  $c = \operatorname{argmax}_k f_\eta(\tilde{y} = k | \mathbf{x})$ . Estimate  $\hat{f}_m$  and  $\hat{f}_m^*$ , the densities of latent variables of easy and hard-minority samples, by KDE.  
Filter out noise samples based on probability densities with thresholds  $\tau$ s and define the selected features of minor set  $\tilde{\mathbf{X}}_m$  as follows:  
$$\tilde{\mathbf{X}}_m = \{\mathbf{x}_i | \hat{f}_m(\mathbf{z}_i) > \tau_1, i \in D_m\} \cup \{\mathbf{x}_i | \hat{f}_m^*(\mathbf{z}_i) > \tau_2, i \in D_m^*\}.$$
  - 11 **Oversampling with SMOTE:**  
 $\hat{\mathbf{X}}_m \leftarrow \tilde{\mathbf{X}}_m$   
**while**  $|\hat{\mathbf{X}}_m| < \rho \cdot |D_M^* \cup D_M|$  **do**
  - 12 |  $\hat{\mathbf{X}}_m \leftarrow \hat{\mathbf{X}}_m \cup \{SMOTE(\mathbf{x})\}, \mathbf{x} \in \tilde{\mathbf{X}}_m$
  - 13 **end**
  - 14 **Return:**  $\hat{\mathbf{X}}_m$

---

## 4.1 Simulation study

We consider a scenario in which the minor class exhibits within-class imbalance that comprises both large and small-sized clusters [1, 41]. The primary challenge

in the small-disjunct problem lies in distinguishing small-sized clusters from noise instances.

To produce our synthetic minority samples, we generate data from two Gaussian distributions as follows:

$$G_1 = \mathcal{N}((-0.3, 0)^\top, \text{diag}(0.01)), G_2 = \mathcal{N}((0.3, 0)^\top, \text{diag}(0.01)).$$

Subsequently, we generate 80 samples from  $G_1$  and 20 samples from  $G_2$ . We generate 1,500 samples from a uniform distribution on  $[-1, 1]^2$  for the major class. Through label-swapping, we artificially generate 50 noise samples from the major set. These noise samples can be regarded as label-contaminated or outliers in the minor group.

Figure 4 (a) displays the samples generated according to our simulation settings, while (b) illustrates a true Bayes decision boundary. In Figure 4 (b), you can observe that samples from  $G_1$  dominate the decision region of the minor class, and the ones from  $G_2$  and noise samples are excluded from the decision region. Through various oversampling methods, we investigate how the decision boundary changes. We conduct a comparative analysis of our proposed method, SMOTE-CLS, against other deep learning approaches, including DFBS [10], DeepSMOTE [11], and DDHS [21] and employ a decision tree as the baseline classifier. To achieve a balanced label ratio, 1400 minority samples are generated by oversampling techniques. The prior distribution of SMOTE-CLS has mean vectors as  $\boldsymbol{\mu}_M = (-1, 1)$ ,  $\boldsymbol{\mu}_m = (1, -1)$ ,  $\boldsymbol{\mu}_{M^*} = (1, 1)$ , and  $\boldsymbol{\mu}_{m^*} = (-1, -1)$ , and variance as  $s_c^2 = 0.1$  for  $c \in \mathcal{Y}^*$ . Additionally, we set  $K = 5$  for the KNN classifier and set  $\tau_1$  and  $\tau_2$  to be selected 90% and 60% samples in  $D_m$  and  $D_m^*$  according to (3.2). XGBoost is employed as the function  $f_\eta$ .

Figure 5 visually represents the oversampling process employed by each step. Specifically, the first row of Figures 5 illustrate the latent space generated by four oversampling methods. Light blue points denote the latent features of the major class, and orange points indicate those of the minor class. Black points are noise variables labeled as the minor class. In Figure 5 (a) and (c), the centroids of the major and the minor classes, which are used in their filtering process, are displayed by the blue and red points, respectively. Unlike the other methods, SMOTE-CLS spatially aligns latent features into four distinct groups based on the predefined priors  $p(\mathbf{z})$  of Figure 2. In the third quadrant of 2 (d), we can see that the noise samples scatter around the minority samples. Therefore, it is visually easy to identify uncommon samples within each group in Figure 5 (d). Most noise samples predominantly consist of hard-minority samples, yet they are noticeably distant from the conditional expectation,  $\boldsymbol{\mu}_{m^*} = (-1, -1)$ .

The second row of Figure 5 visualizes the latent variables ( $\mathbf{z}$ ) after each filtering process, and the third row of Figure 5 shows the filtered minor set ( $\tilde{\mathbf{X}}_m$ ). Note that  $\mathbf{z}$  denotes the latent variables without specifying a particular model. Only DeepSMOTE does not have its filtering process such that Figure 5 (b) is equal to Figure 5 (f). First, DFBS defines the candidate set for oversampling, which satisfies the following condition:

$$\tilde{\mathbf{X}}_m = \{\mathbf{x}_i \mid \|\mathbf{z}_i - \bar{\mathbf{z}}_M\| > \|\mathbf{z}_i - \bar{\mathbf{z}}_m\|, y_i = m\},$$

where  $\bar{\mathbf{z}}_M$  and  $\bar{\mathbf{z}}_m$  denote the centers of latent variables of major and minor sets, respectively, presented as green and red points in Figure 5 (a).

The center of each class computed with Euclidean distance is biased to outliers or large-sized clusters. Therefore, as shown in Figures 5 (e) and (i), the selected latent variables and minority samples predominantly come from the large-sized cluster, and even noise samples near the large-sized cluster are chosen. This outcome is because the center of the minor class is slightly biased toward the large-sized cluster. Consequently, the latent variables from the small-sized cluster are excluded from the candidate set for oversampling.

Figures 5 (f) and (j) pertain to DeepSMOTE, which does not involve a filtering process; it selects all minority samples, including noise ones, as candidates. Because of the unconditional oversampling, its decision boundary in Figure 5 (n) is not a desired result.

Especially, DDHS selects the minor subset for oversampling and the major subset for training the classifier based on the probability densities. In this paper, we only focus on the selection of a minor subset, and its filtering algorithm for only the minor set can be written as follows:

$$\tilde{\mathbf{X}}_m = \{\mathbf{x}_i \mid \hat{f}_{m,m^*}(\mathbf{z}_i) > \tau_3, y_i = m\},$$

where  $\hat{f}_{m,m^*}$  is an estimated density of minor latent variables by KDE, and set  $\tau_3$  to select 75% minor samples. In a similar way, DDHS selects the 50% major samples by  $\hat{f}_{M,M^*}$

In Figure 5 (g) and (k), corresponding to the results of DDHS, only minority samples with higher densities in the latent space are selected. As a result, samples from the small and large clusters are excluded from the candidate set for oversampling. Additionally, DDHS keeps the minority samples not selected for oversampling to train the classifier while excluding the major ones not selected. As a result, in Figure 5 (o), noise samples dominate the decision boundary region where the major samples have been removed.

In contrast, as shown in Figures 5 (h) and (l), SMOTE-CLS effectively filters out noise samples from the minor class while also selecting candidates from both the large and small-sized clusters. Precisely, in our approach, we consider both similarity and difficulty when embedding samples into the latent space. This results in more balanced and effective oversampling, as the selected latent variables include representatives from both clusters rather than being dominated by samples from the larger cluster. This approach allows us to generate synthetic samples that better capture the underlying distribution of the minor class, ultimately improving classification performance.

Finally, the last row of Figures 5 represents the oversampling outcomes with augmented minor set  $\hat{\mathbf{X}}_m$  on the data space. DFBS and DeepSMOTE appear susceptible to noise samples, while DDHS fails to augment samples from the  $G_2$  because the filtering process excludes the small disjunct population. In contrast, only SMOTE-CLS exhibits a decision boundary that closely aligns with the true generative models

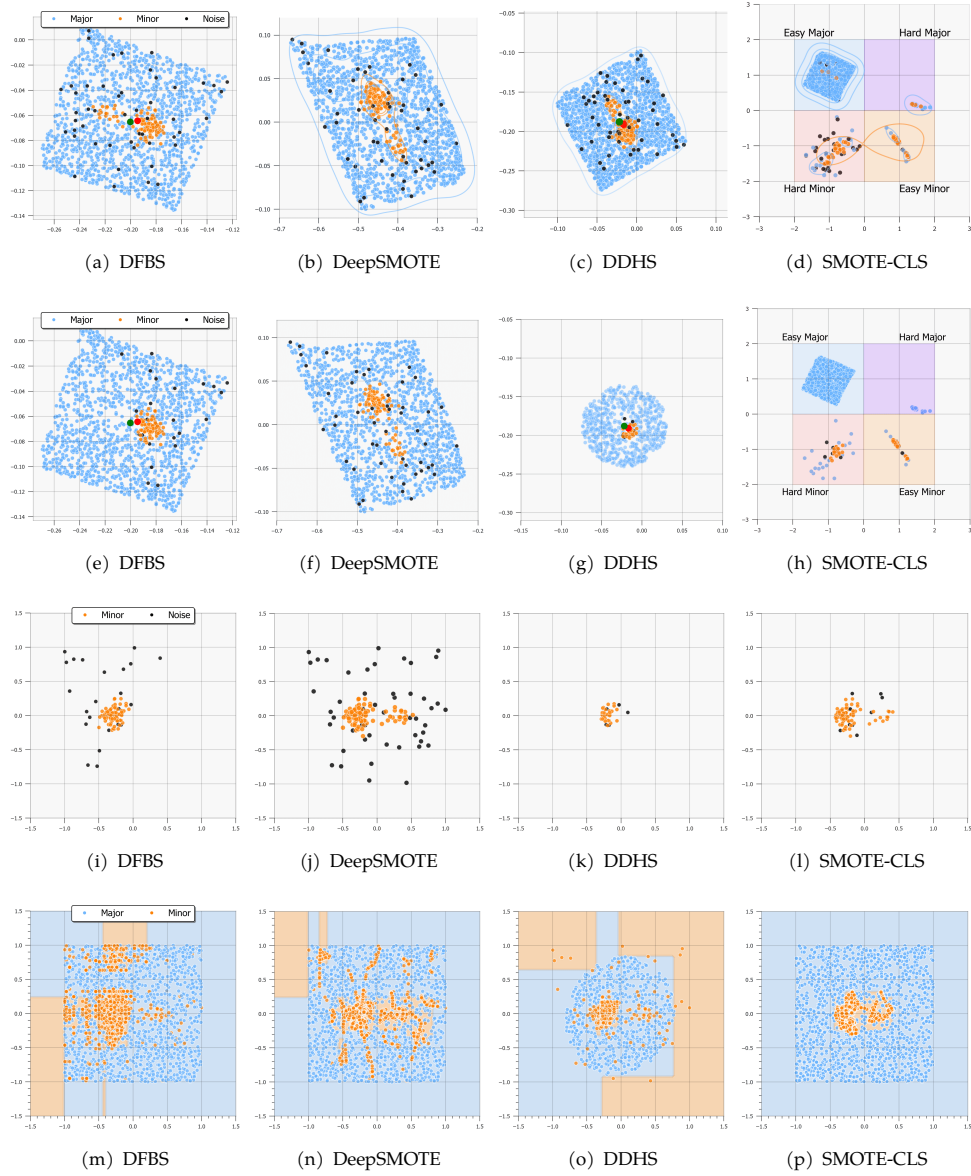


**Fig. 5** Visualization of the oversampling process in the simulation study. (a) - (d): the trained latent variables. (e) - (h): the selected latent variables by each filtering method. (i) - (l): the selected minority samples for oversampling. (m) - (p): the oversampling results and decision boundary using decision trees. In the visual representation of DFBS and DDHS, green and red points denote the centers of major and minor sets, respectively. Note that the centers of each class do not exhibit a clear separation.

$G_1$  and  $G_2$ . Through this simulation study, SMOTE-CLS has robustness to noise and outperforms other oversampling methods in within-class imbalance classification.

**Table 1** Summary of the models in the ablation study.

Model	Disentanglement	Difficulty segmentation	Adaptive filtering
w/o dis	✗	✗	✗
w/o seg	✓	✗	✗
w/o af	✓	✓	✗
SMOTE-CLS	✓	✓	✓

## 4.2 Ablation Studies

We conduct ablation studies to assess the significance of each step in Algorithm 1. With the synthetic data used in Section 4.1 we demonstrate its ability to filter out noise and select high-quality candidates for oversampling effectively. Our study focuses on three key aspects of the proposed procedure: disentangling latent space (the use of GMM), sample difficulty segmentation (introduction of refined levels in (1)), and group adaptive filtering (Section 3.2). Each step is configured, and the generated minority samples in the configured SMOTE-CLS are compared.

Table 1 shows the configuration in the ablation study. The ‘w/o dis’ model denotes the VAE without disentangling the latent space, essentially equivalent to the conditional VAE (CVAE). The ‘w/o seg’ model represents the VAE that disentangles the major and minor groups without incorporating the segmentation according to classification difficulty. In this case, we employ the two-component Gaussian mixture distribution as the prior and set the location parameters of each class as  $(1, 1)$  for the major class and  $(-1, -1)$  for the minor class.

The ‘w/o af’ model denotes the SMOTE-CLS model, excluding the group adaptive filtering. It’s worth noting that the other models, excluding SMOTE-CLS, involve the naive density-based filtering algorithm, which employs KDE on the entire minor set and selects a minority sample whose density is higher than a predefined threshold  $\tau$ . In this study, we set  $\tau$  where 40% of the minority samples are filtered out.

Each column of Figure 6 corresponds to the configuration in the SMOTE-CLS for the ablation study. The last column shows the result of the SMOTE-CLS. Each row from top to bottom illustrates the latent variables, the filtered latent variables, and the filtered data points of the minor class. Thus, the bottom row displays what minority samples are selected as high-quality samples under the small disjunct problem existing.

In the first column in Figure 6, the latent space of ‘w/o dis’ is similar to the other AE-based models, such as DFBS, DDHS, and DeepSMOTE, in Figure 5 that exploits only class labels without additional information or disentangling latent space. As a result, the noise samples, mislabelled data following the major class distribution, are embedded around the minor class, and the samples from the small disjunct are ignored by ‘w/o dis’. See Figure 6 (i).

As seen in Figure 6 (b), when the sample difficulty segmentation is not applied, a significant amount of minority samples are embedded around  $(1, 1)$ , the center of the prior of the major class. Conversely, noise samples are embedded around  $(1, 1)$ , the

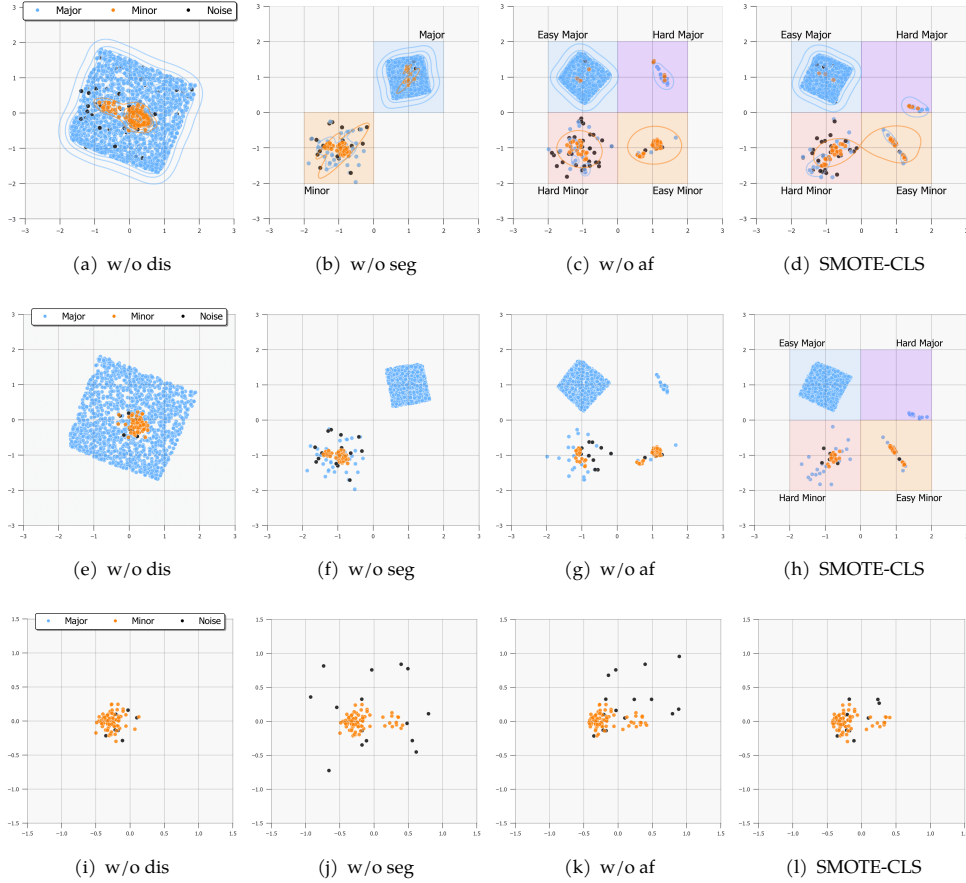


**Fig. 6** Visualization of the ablation study. (a) - (d): the trained latent variables. (e) - (h): the selected latent variables by each filtering method. (i) - (l): the selected minority samples for oversampling.

center of the prior of the minor class. It leads to undesirable outcomes in the density-based filtering process because these minority samples are excluded. In contrast, many noise samples are selected, as shown in Figures 6 (f) and (j).

In the case of ‘w/o af’ denoting SMOTE-CLS without the group adaptive filtering algorithm, the latent spaces of hard and easy samples are divided by the predefined prior distribution in Figure 6 (c). In contrast to Figure 6 (b), the minority samples are embedded within the latent space of both hard and easy-minor sets, forming a bimodal distribution. However, the filtering with the KDE cannot exclude the noise samples from the minor class because the noise samples are embedded with the minority samples. The latent variables of noise samples are close to the distribution of the easy-minor class. This happens because these noise samples have higher densities than the minority samples that are farther from the prior distribution of the easy-minor class. See Figures 6 (g) and (k).



Table 2 Summary of the datasets.

Dataset	Repository	# samples	# features	IR
ecoli	UCI	336	7	11.6% (301:35)
libras_move	UCI	360	90	7.1% (336:24)
spectrometer	UCI	531	93	9.3% (486:45)
oil	UCI	937	49	4.6% (896:41)
yeast	UCI	1,484	8	3.6% (1433:51)
car_eval	UCI	1,728	21	8.4% (1594:134)
us_crime	UCI	1,994	100	8.1% (1844:150)
scene	LIBSVM	2,407	294	7.9% (2230:177)
abalone	UCI	4,177	10	10.3% (3786:391)
optical_digits	UCI	5,620	64	10.9% (5066:554)
satimage	UCI	6,435	36	10.8% (5809:626)
isolet	UCI	7,797	617	8.3% (7197:600)

These results highlight the need for our proposed method to effectively address challenging issues, such as noise filtering and the selection of small-sized minor sets. Also, contrary to ‘w/o af’, our proposed model is robust to the prior distribution (see Appendix A2). Note that SMOTE-CLS does not provide only a statistical detection method for a noise sample. Instead, it renders a general method of specifying a local neighborhood on data space  $\mathcal{X}$  via the disentanglement of latent space  $\mathcal{Z}$ . SMOTE-CLS constructs clusters on latent variables via the prior distribution, the predesigned GMM aiming to a specific disentanglement. By relabeling observations, we can separate each mode of  $q(\mathbf{z}|\hat{y} = c)$  for  $c = M^*, m^*, M, m$  and define a cluster within each subclass. The samples in each cluster convey information about a new neighborhood used in SMOTE. Furthermore, because the criterion of the disentanglement can be variously defined according to the object of data analysis, SMOTE-CLE provides a flexible way to define a neighborhood for improving SMOTE.

### 4.3 Real Data Analysis

#### 4.3.1 Datasets

We conduct a comparative study with 12 benchmark imbalanced datasets. These datasets are publicly available in the UCI Machine Learning Repository [42] and the LIBSVM dataset repository [43]. Table 2 provides detailed descriptions of the benchmark datasets, including the number of samples (ranging from 336 to 7797), the number of features (ranging from 7 to 617), and the imbalanced ratio (IR). IR is calculated as the ratio of the major class size to the minor class size and varies from 3.6% to 11.6%.

#### 4.3.2 Comparison Models

Our experiments compare SMOTE-CLS with 9 benchmarks, including SMOTE-based and deep learning-based approaches. Along with the comparative models used in Section 4.2, we consider five additional models: Baseline (BASE) without oversampling, SMOTE, Borderline-SMOTE (BSMOTE), SMOTE-ENN, KSMOTE,

**Table 3** Summary of the oversampling techniques.

Model	Reference	Methods
BASE	-	without oversampling
SMOTE	[5]	SMOTE
BSMOTE	[8]	SMOTE + filtering
SMOTE-ENN	[28]	SMOTE + filtering
KMSMOTE	[29]	SMOTE + cluster-based filtering
DFBS	[10]	Autoencoder + distance-based filtering + feature random combination
DeepSMOTE	[11]	Autoencoder + SMOTE on latent variables
DDHS	[21]	Autoencoder + KDE-based filtering + feature random combination
CVAE	[18]	Conditional VAE
SMOTE-CLS	Ours	VAE with customized latent space + KDE-based filtering + SMOTE

and CVAE. The SMOTE-based methods are implemented using the imbalanced-learn package [44]. The summary of the models is described in Table 3.

### 4.3.3 Evaluation Metrics

This study uses the Area Under the Precision-Recall Curve (AUPRC) and the Area Under the Curve (AUC) as our evaluation metrics. The AUPRC provides a comprehensive metric by considering Precision-Recall pairs across various thresholds, which is particularly valuable in the context of highly imbalanced classes. The definitions of precision and recall are as follows:

$$\text{Precision} = \frac{TP}{TP + FP}$$

$$\text{Recall} = \frac{TP}{TP + FN'}$$

where  $TP$ ,  $FP$ , and  $FN$  denote the number of positive class samples correctly predicted by the classifier as a positive class, the number of negative class samples incorrectly predicted by the classifier as a positive class, and the number of positive class samples incorrectly predicted by the classifier as a negative class, respectively. In this study, we let the minor class be the positive. We also report the AUC, a general metric for assessing classification performance, taking into account all thresholds on the receiver operating characteristic curve. Both metrics are not dependent on a classification threshold value, thus being capable of measuring overall performance. Especially in imbalanced datasets, AUPRC is more informative than AUC [45, 46].

### 4.3.4 Experimental Design

We randomly split the datasets into training and test sets with an 8:2 ratio. Subsequently, the minority samples are augmented in the training set by each oversample method. We set the balanced dataset’s oversampling ratio  $\rho = 1$ , ensuring an equal

number of minor and major samples. To evaluate the oversampling method, we fit a classifier with the augmented training set and measure evaluation metrics using the test set. The above process is repeated ten times, and the mean and standard errors of the evaluation metrics are reported. Our experiments employ the random forest as our baseline classifier.

For the training process of SMOTE-CLS, we configure the dimension of the latent variable to be 4 for datasets with more than 90 features and 2 for the remaining datasets. Suppose we denote the dimension of the latent variable as  $h \in \{2, 4\}$ . In that case, the architecture of the encoder and decoder are designed by the feedforward network with the dimension of the hidden layers given by  $(8h, 4h, 2h, h, 2h, 4h, 8h)$  in order. The prior distribution of SMOTE-CLS is characterized by mean vectors:  $\boldsymbol{\mu}_M = (-1, 1)$ ,  $\boldsymbol{\mu}_m = (1, -1)$ ,  $\boldsymbol{\mu}_{m^*} = (-1, -1)$ , and  $\boldsymbol{\mu}_{M^*} = (1, 1)$ , and variance:  $s_c^2 = 0.1$  for  $c \in \mathcal{Y}^*$ . Like the simulation study, we set  $K = 5$  for the KNN classifier  $f_K$  and employ XGBoost as  $f_\eta$  in (3).

### 4.3.5 Experimental Results

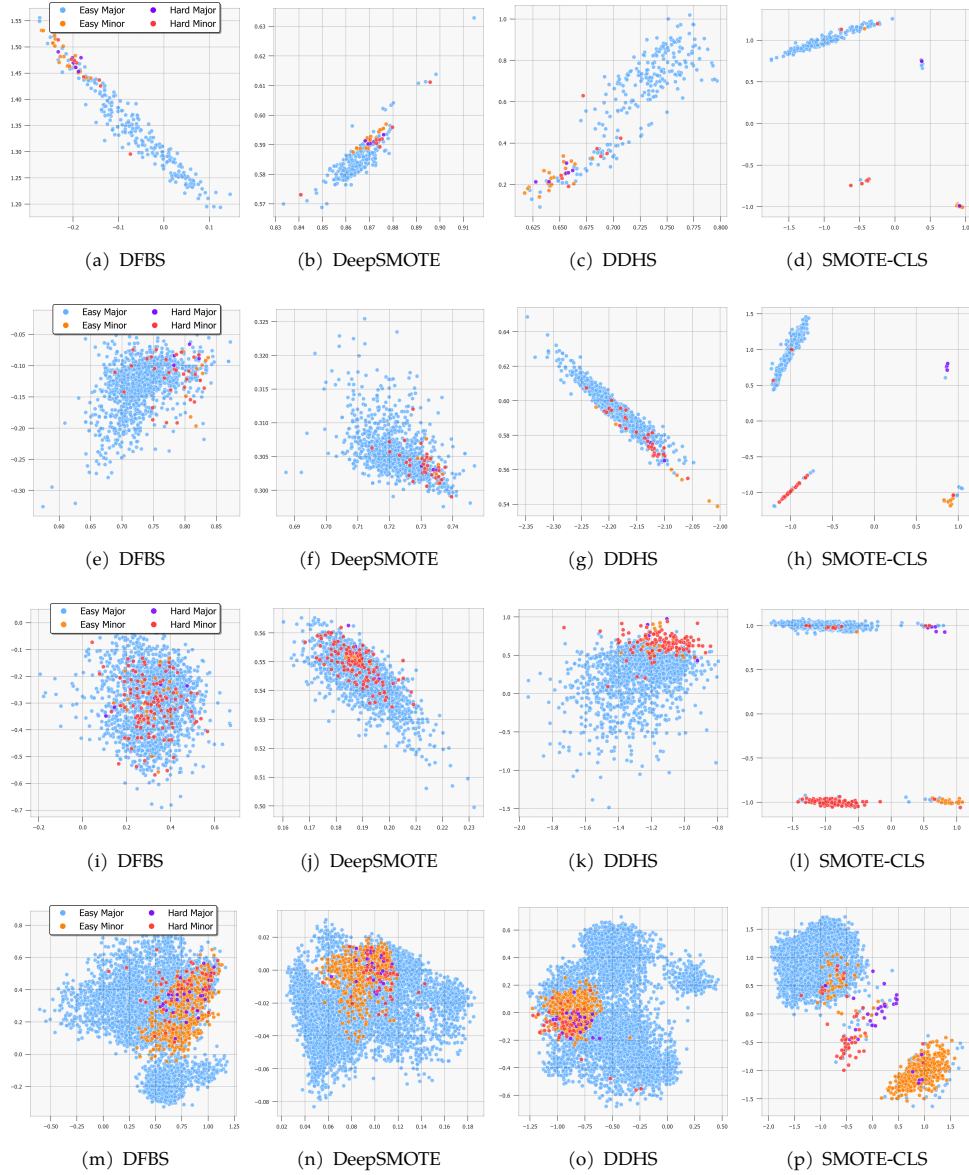
Table 4 summarizes the average AUPRC and standard error of 10 repeated experiments. Regarding imbalanced classification performance, SMOTE-CLS exhibits consistently better performance than other methods, regardless of whether the datasets have low or high imbalance ratios. SMOTE-CLS is the top-performing method in 7 out of 12 datasets, with an average ranking of 2.08. It’s noteworthy that SMOTE-CLS consistently outperforms SMOTE across all datasets, confirming its ability to address the weaknesses of SMOTE and enhance its performance. Additionally, our proposed model demonstrates its effectiveness, particularly in high-dimensional datasets like scene and isolet, outperforming deep learning approaches.

Table 5 summarizes the average AUC and standard error of 10 repeated experiments. When assessing overall classification performance, SMOTE-CLS consistently ranks among the top-performing models, with an average ranking of 3.00. It is worth noting that the SMOTE-based oversampling methods, including our proposed SMOTE-CLS, outperform the deep learning methods in terms of AUC. This observation verifies that the samples generated by SMOTE-based methods are more effective than those generated by deep learning methods in the benchmark dataset.

Our real data analysis demonstrates that SMOTE-CLS significantly enhances minor labels (or positive samples) while maintaining a solid overall classification performance. Additionally, the comparison with SMOTE and BSMOTE on average performance highlights that simple filtering algorithms, like those used in BSMOTE, may not be as effective as our data-adaptive filtering in handling imbalanced classification tasks. These results justify the importance of our approach, which takes into account the data’s characteristics to elaborate decisions about filtering and oversampling. For additional performance metrics, please refer to Appendix A4.

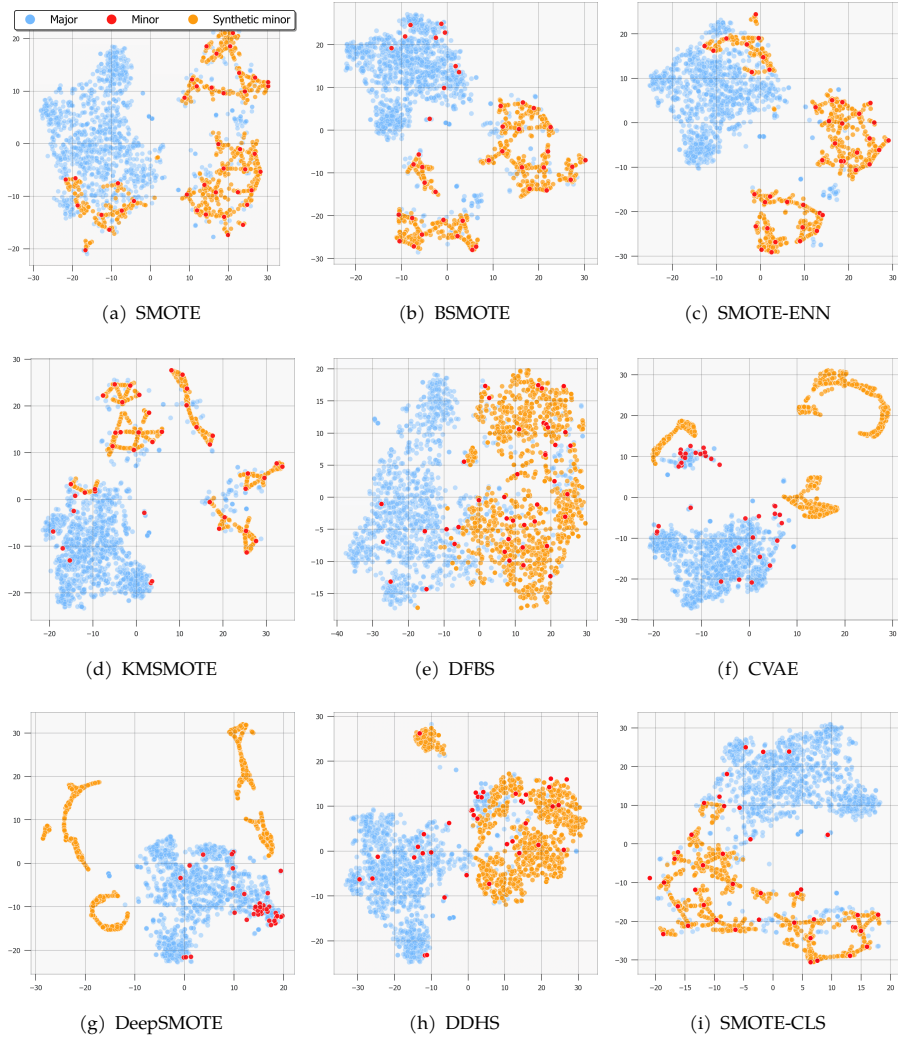
### 4.3.6 Visualizations

Figure 7 shows the latent spaces of DFBS, DeepSMOTE, DDHS, and SMOTE-CLS for four datasets: the first row for *ecoli*, the second row for *yeast*, the third row



**Fig. 7** Visualization of latent spaces for 4 datasets: (a) - (d): *ecoli* dataset, (e) - (h): *yeast* dataset, (i) - (l): *scene* dataset, (m) - (p): *isolet* dataset. The assignment of labels is determined by the KNN classifier  $f_K$ . In the case of SMOTE-CLS, the noise samples are identified using our filtering algorithm and subsequently removed from the training set.

for *scene*, and the last row for *isolet*. The colors of the points represent the sample difficulty as determined by the KNN classifier  $f_K$ . In low-dimensional datasets like *ecoli*, the latent space of all models shows distinctive features for each class.



**Fig. 8** t-SNE plots of the augmented yeast dataset by oversampling methods with  $\rho = 1.0$ .

However, in the high-dimensional datasets (`scene` and `isolet`), latent variables of DFBS, DeepSMOTE, and DDHS are overlapped among the four classes. On the other hand, SMOTE-CLS exhibits a relatively more distinct latent space with the augmented labels. It is worth noting that the latent visualizations provided by SMOTE-CLS effectively aid in noise identification, allowing us to determine the appropriate threshold  $\tau$  for filtering it out.

Figure 8 displays the t-SNE plots [47] of the augmented yeast dataset. Figure 8 (a) shows that SMOTE is prone to noise samples, which is undesirable. Figure 8 (c) SMOTE-ENN seems to mitigate the problem of generating minority samples around noise samples. However, when a high oversampling ratio is used, such as

$\rho = 1.0$  in our setup, a significant number of generated samples forms a cluster, and SMOTE-ENN fails to filter out noise samples effectively. Consequently, SMOTE-ENN yields similar results to those of SMOTE. However, both BSMOTE (Figure 8 (b)), KMSMOTE (Figure 8 (d)), and SMOTE-CLS (Figure 8 (i)) filter them out in the candidates for oversampling. In addition, BSMOTE, while conservative, tends to overlook small disjuncts of the minor class within the major class. In contrast, our approach can identify these small disjuncts without clustering. Furthermore, KMSMOTE, which generates synthetic minority samples within clusters using SMOTE, has the potential drawback of reducing sample diversity and being sensitive to the results of the clustering process. In the context of deep learning approaches, specifically CVAE (Figure 8 (f)) and DeepSMOTE (Figure 8 (g)), which directly employ the decoder to generate minority samples, there is a tendency to produce low-quality samples due to their limited reconstruction ability. Regarding DFBS (Figure 8 (e)) and DDHS (Figure 8 (h)), which employ their generation techniques, they generate various minority samples. However, these samples often overlap with the major class regions, negatively impacting classification performance.

## 5 Conclusions and Limitations

In this study, we proposed a novel oversampling algorithm, SMOTE-CLS, which exploits the strengths of SMOTE and VAE. Our algorithm comprises four key steps: classifying sample difficulty, training VAE with a tailored latent space, applying density-based filtering, and oversampling using SMOTE. Through numerical studies with the synthetic data, we demonstrated the necessity of each step in improving the SMOTE algorithm and superiority over the existing methods. In real data analysis, SMOTE-CLS significantly improved classification performance for the minor class, as measured by the AUPRC. Moreover, the visualization results provided empirical evidence of SMOTE-CLS’s ability to generate high-quality minority samples and its robustness to noise. Additionally, we anticipate that our filtering algorithm can seamlessly integrate with other state-of-the-art oversampling methods, further enhancing its versatility and applicability.

One intriguing finding was elucidated through the current investigation: the substantial impact of data generation capability via neural network models on enhancing the predictive performance of minor class augmentation. Specifically, the augmented minority samples, while effectively distinguished from majority samples, show distinct characteristics compared to the original minor class data and occasionally degrade the classification models’ predictive efficacy. Conversely, by augmenting samples within the data space, SMOTE ensured that the augmented samples have features more akin to the observed minority samples. In essence, for minor class data augmentation, the quantity of data pertinent to the minor class, rather than that of the whole dataset, proved crucial. Especially for sparse data, augmenting directly within the data space, as facilitated by techniques like SMOTE, which define and augment neighbors, exhibited superior augmentation performance over neural network-based generative models that struggle with data reproducibility.

Even though SMOTE-CLS showed superior performance compared to other oversampling methods, it still has some limitations. One notable limitation is its applicability to multi-class tasks, as customizing the latent space based on the confusion matrix can be challenging in such scenarios. While one potential solution could involve utilizing a higher-dimensional latent space, it is essential to consider that this approach may present challenges to the effectiveness of the density-based filtering algorithm, particularly in higher-dimensional settings. Some possible solutions extending the applicability of our approach include leveraging prior knowledge of label relationships and developing methods to map such relationships to the latent space. One approach could involve learning the prior distribution rather than fixing it to maximize the distance among classes, as proposed by [48]. We leave them as our future works.

## References

- [1] He, H., Garcia, E.A.: Learning from imbalanced data. *IEEE Transactions on knowledge and data engineering* **21**(9), 1263–1284 (2009)
- [2] Mazurowski, M.A., Habas, P.A., Zurada, J.M., Lo, J.Y., Baker, J.A., Tourassi, G.D.: Training neural network classifiers for medical decision making: The effects of imbalanced datasets on classification performance. *Neural networks* **21**(2-3), 427–436 (2008)
- [3] Malhotra, R., Kamal, S.: An empirical study to investigate oversampling methods for improving software defect prediction using imbalanced data. *Neurocomputing* **343**, 120–140 (2019)
- [4] Idakwo, G., Thangapandian, S., Luttrell, J., Li, Y., Wang, N., Zhou, Z., Hong, H., Yang, B., Zhang, C., Gong, P.: Structure–activity relationship-based chemical classification of highly imbalanced tox21 datasets. *Journal of cheminformatics* **12**(1), 1–19 (2020)
- [5] Chawla, N.V., Bowyer, K.W., Hall, L.O., Kegelmeyer, W.P.: Smote: synthetic minority over-sampling technique. *Journal of artificial intelligence research* **16**, 321–357 (2002)
- [6] Fernández, A., Garcia, S., Herrera, F., Chawla, N.V.: Smote for learning from imbalanced data: progress and challenges, marking the 15-year anniversary. *Journal of artificial intelligence research* **61**, 863–905 (2018)
- [7] Kovács, G.: Smote-variants: A python implementation of 85 minority oversampling techniques. *Neurocomputing* **366**, 352–354 (2019)
- [8] Han, H., Wang, W., Mao, B.: Borderline-smote: A new over-sampling method in imbalanced data sets learning. In: *International Conference on Intelligent Computing* (2005)

- [9] He, H., Bai, Y., Garcia, E.A., Li, S.: Adasyn: Adaptive synthetic sampling approach for imbalanced learning. In: 2008 IEEE International Joint Conference on Neural Networks (IEEE World Congress on Computational Intelligence), pp. 1322–1328 (2008). Ieee
- [10] Liu, Y., Liu, C.-L., Tseng, V.S.: Deep discriminative features learning and sampling for imbalanced data problem. 2018 IEEE International Conference on Data Mining (ICDM), 1146–1151 (2018)
- [11] Dablain, D., Krawczyk, B., Chawla, N.V.: Deepsmote: Fusing deep learning and smote for imbalanced data. IEEE Transactions on Neural Networks and Learning Systems **34**(9), 6390–6404 (2023)
- [12] Shin, K., Kang, S.: Adanoise: Training neural networks with adaptive noise for imbalanced data classification. Expert Systems with Applications **192**, 116364 (2022)
- [13] Tian, J., Chen, S., Zhang, X., Feng, Z., Xiong, D., Wu, S., Dou, C.: Re-embedding difficult samples via mutual information constrained semantically oversampling for imbalanced text classification. In: Proceedings of the 2021 Conference on Empirical Methods in Natural Language Processing, pp. 3148–3161 (2021)
- [14] Dablain, D.A., Bellinger, C., Krawczyk, B., Chawla, N.V.: Efficient augmentation for imbalanced deep learning. In: 2023 IEEE 39th International Conference on Data Engineering (ICDE), pp. 1433–1446 (2023). IEEE
- [15] Kingma, D.P., Welling, M.: Auto-encoding variational bayes. arXiv preprint arXiv:1312.6114 (2013)
- [16] Goodfellow, I., Pouget-Abadie, J., Mirza, M., Xu, B., Warde-Farley, D., Ozair, S., Courville, A., Bengio, Y.: Generative adversarial nets. Advances in neural information processing systems **27** (2014)
- [17] Dai, W., Ng, K., Sevenson, K.A., Huang, W., Anderson, F., Stultz, C.M.: Generative oversampling with a contrastive variational autoencoder. 2019 IEEE International Conference on Data Mining (ICDM), 101–109 (2019)
- [18] Fajardo, V.A., Findlay, D., Jaiswal, C., Yin, X., Houmanfar, R., Xie, H., Liang, J., She, X., Emerson, D.: On oversampling imbalanced data with deep conditional generative models. Expert Systems with Applications **169**, 114463 (2021)
- [19] Camino, R.D., Hammerschmidt, C.A.: Oversampling tabular data with deep generative models: Is it worth the effort? In: ICBINB@NeurIPS (2020)
- [20] Nakai, K.: Ecoli. UCI Machine Learning Repository. DOI: <https://doi.org/10.24432/C5388M> (1996)



- [21] Liu, C.-L., Chang, Y.: Learning from imbalanced data with deep density hybrid sampling. *IEEE Transactions on Systems, Man, and Cybernetics: Systems* **52**, 7065–7077 (2022)
- [22] Azhar, N.A., Pozi, M.S.M., Din, A.M., Jatowt, A.: An investigation of smote based methods for imbalanced datasets with data complexity analysis. *IEEE Transactions on Knowledge and Data Engineering* (2022)
- [23] Van Kerm, P.: Adaptive kernel density estimation. *The Stata Journal* **3**(2), 148–156 (2003)
- [24] An, S., Jeon, J.-J.: Customization of latent space in semi-supervised variational autoencoder. *Pattern Recognition Letters* **177**, 54–60 (2024)
- [25] Liu, T., Qian, Z., Berrevoets, J., Schaar, M.: GOGGLE: Generative modelling for tabular data by learning relational structure. In: *The Eleventh International Conference on Learning Representations* (2023)
- [26] Kamalov, F.: Kernel density estimation based sampling for imbalanced class distribution. *Information Sciences* **512**, 1192–1201 (2020)
- [27] Elreedy, D., Atiya, A.F., Kamalov, F.: A theoretical distribution analysis of synthetic minority oversampling technique (smote) for imbalanced learning. *Machine Learning*, 1–21 (2023)
- [28] Batista, G.E., Prati, R.C., Monard, M.C.: A study of the behavior of several methods for balancing machine learning training data. *ACM SIGKDD explorations newsletter* **6**(1), 20–29 (2004)
- [29] Douzas, G., Bacao, F., Last, F.: Improving imbalanced learning through a heuristic oversampling method based on k-means and smote. *Information Sciences* **465**, 1–20 (2018)
- [30] Wen, Y., Zhang, K., Li, Z., Qiao, Y.: A discriminative feature learning approach for deep face recognition. In: *Computer Vision–ECCV 2016: 14th European Conference, Amsterdam, The Netherlands, October 11–14, 2016, Proceedings, Part VII 14*, pp. 499–515 (2016). Springer
- [31] Solomon, I., Jayavelu, S., Ferdous, M.M., Kumar, U.: Data oversampling with structure preserving variational learning. In: *Proceedings of the 31st ACM International Conference on Information & Knowledge Management*, pp. 4490–4494 (2022)
- [32] Sorscher, B., Geirhos, R., Shekhar, S., Ganguli, S., Morcos, A.: Beyond neural scaling laws: beating power law scaling via data pruning. *Advances in Neural Information Processing Systems* **35**, 19523–19536 (2022)

- [33] Sohn, K., Lee, H., Yan, X.: Learning structured output representation using deep conditional generative models. *Advances in neural information processing systems* **28** (2015)
- [34] Breiman, L.: Random forests. *Machine learning* **45**, 5–32 (2001)
- [35] Chen, T., Guestrin, C.: Xgboost: A scalable tree boosting system. *Proceedings of the 22nd ACM SIGKDD International Conference on Knowledge Discovery and Data Mining* (2016)
- [36] Xie, Y., Qiu, M., Zhang, H., Peng, L., Chen, Z.: Gaussian distribution based oversampling for imbalanced data classification. *IEEE Transactions on Knowledge and Data Engineering* **34**(2), 667–679 (2020)
- [37] Achlioptas, P., Diamanti, O., Mitliagkas, I., Guibas, L.: Learning representations and generative models for 3D point clouds. In: Dy, J., Krause, A. (eds.) *Proceedings of the 35th International Conference on Machine Learning. Proceedings of Machine Learning Research*, vol. 80, pp. 40–49. PMLR, ??? (2018)
- [38] Dai, B., Wipf, D.: Diagnosing and enhancing VAE models. In: *International Conference on Learning Representations* (2019)
- [39] Scott, D.W.: On optimal and data based histograms. *Biometrika* **66**, 605–610 (1979)
- [40] Ghosh, A.K., Chaudhuri, P.: Optimal smoothing in kernel discriminant analysis. *Statistica Sinica*, 457–483 (2004)
- [41] Liu, R.: A novel synthetic minority oversampling technique based on relative and absolute densities for imbalanced classification. *Applied Intelligence* **53**(1), 786–803 (2023)
- [42] Markelle Kelly, K.N. Rachel Longjohn: *The UCI Machine Learning Repository* (2023)
- [43] Chang, C.-C., Lin, C.-J.: Libsvm: a library for support vector machines. *ACM transactions on intelligent systems and technology (TIST)* **2**(3), 1–27 (2011)
- [44] Lemaître, G., Nogueira, F., Aridas, C.K.: Imbalanced-learn: A python toolbox to tackle the curse of imbalanced datasets in machine learning. *The Journal of Machine Learning Research* **18**(1), 559–563 (2017)
- [45] Davis, J., Goadrich, M.: The relationship between precision-recall and roc curves. In: *Proceedings of the 23rd International Conference on Machine Learning*, pp. 233–240 (2006)
- [46] Hancock, J.T., Khoshgoftaar, T.M., Johnson, J.M.: Evaluating classifier performance with highly imbalanced big data. *Journal of Big Data* **10**(1), 42 (2023)

- [47] Maaten, L., Hinton, G.: Visualizing data using t-sne. *Journal of machine learning research* **9**(11) (2008)
- [48] Hajimiri, S., Lotfi, A., Baghshah, M.S.: Semi-supervised disentanglement of class-related and class-independent factors in vae. *arXiv preprint arXiv:2102.00892* (2021)

## Appendix A Effect of the classifier $f_\eta$ on customizing latent space

In Section 3, we emphasize the importance of exploiting the superior performance of the tree-based classifier. Figure A1 presents the visual representation of the filtering processes using a multilayer perceptron and XGBoost for  $f_\eta$ . ‘MLP’ employs the multilayer perceptron for the  $f_\eta$  function, and ‘XGB’ denotes the proposed SMOTE-CLS with XGBoost for  $f_\eta$ . Comparing Figures A1 (a) and (d), it demonstrates that utilizing the XGBoost classifier significantly enhances the disentanglement of the latent space, particularly concerning augmented labels,  $\mathcal{Y}^*$ . Furthermore, it’s important to note that poor disentanglement can lead to lower interpretability. These findings underscore the pivotal role of our approach, which leverages a tree-based classifier to utilize its classification capabilities, aligning with our goals.

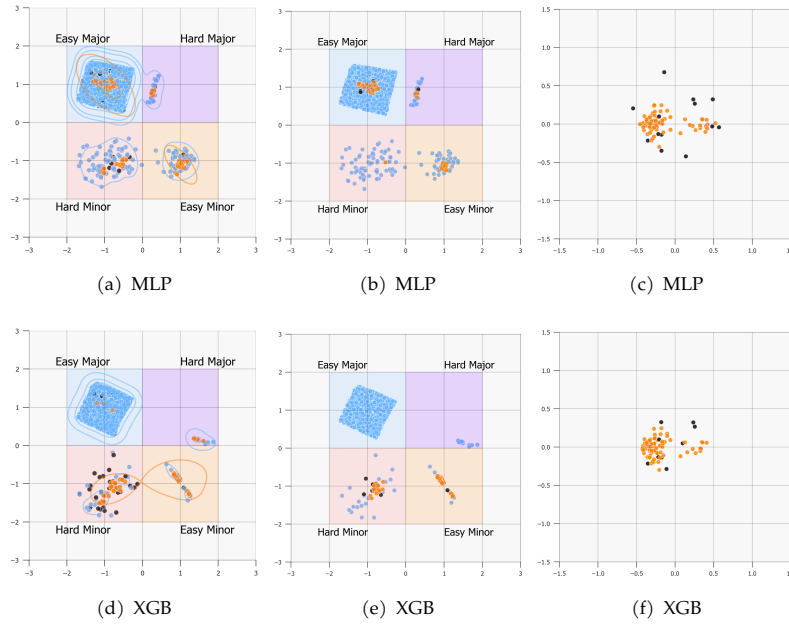


**Fig. A1** Visualization of the effect of classifier on the latent space. (a) and (d): the trained latent variables. (b) and (e): the selected latent variables by filtering method. (c) and (f): the selected minority samples for oversampling.

## Appendix B Effects of prior distribution

We investigate the effects of location parameters of the prior. Figure B2 visually represents the filtering process using SMOTE-CLS with different prior settings. Each colored square represents the predefined area for each group. ‘SMOTE-CLS1’ presents SMOTE-CLS used in Section 4.1 and 4.2. In ‘SMOTE-CLS2’, we adjust the distances within each class to be greater than one between classes. For ‘SMOTE-CLS3’, we allocate the x-axis to represent difficulty and the y-axis to denote class. In ‘SMOTE-CLS4’, we set the same location parameters for hard and easy samples of each class. As illustrated in Figures B2 (i) - (l), our methods are robust to the selection of the prior.

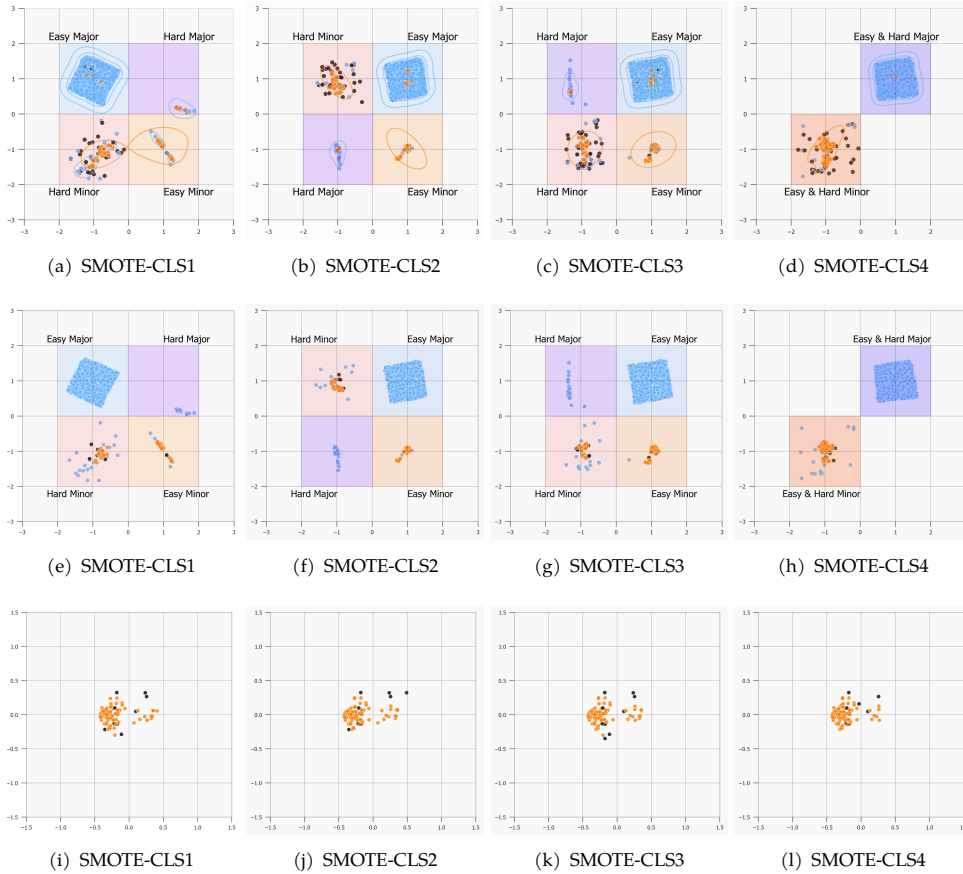


**Fig. B2** Visualization of the ablation study. (a) - (d): the trained latent variables. (e) - (h): the selected latent variables by each filtering method. (i) - (l): the selected minority samples for oversampling.

## Appendix C Visualization of the latent space with the threshold $\tau_s$

In the process of group-adaptive filtering described in Equation (3.2), noise identification depends on the choice of tuning parameters, denoted as  $\tau_1$  and  $\tau_2$ . To investigate how to select these tuning parameters effectively, we turn to visual representations using the simulation data from Section 4.1. For simplicity, we set  $\tau_1$  to be selected 10% samples in  $D_m$  and then explore different values of  $\tau_2$  to be selected 30%, 50%, and 70% samples in  $D_m^*$ . The first row of Figure C3 displays the latent variables selected by varying  $\tau_2$ , without labeling noise in practice. This visual exploration helps us determine an appropriate choice for  $\tau_2$ . In Figures C3 (a) and (b), some hard minority samples that are selected appear to be distant from their centers, suggesting they may be noise. Conversely, in Figure C3 (c), all hard-minority samples are clustered around their center. This observation suggests that selecting 30% of  $D_m^*$  could be considered an optimal parameter choice. The second row of Figure C3 illustrates the selected minority samples based on  $\tau_2$ .

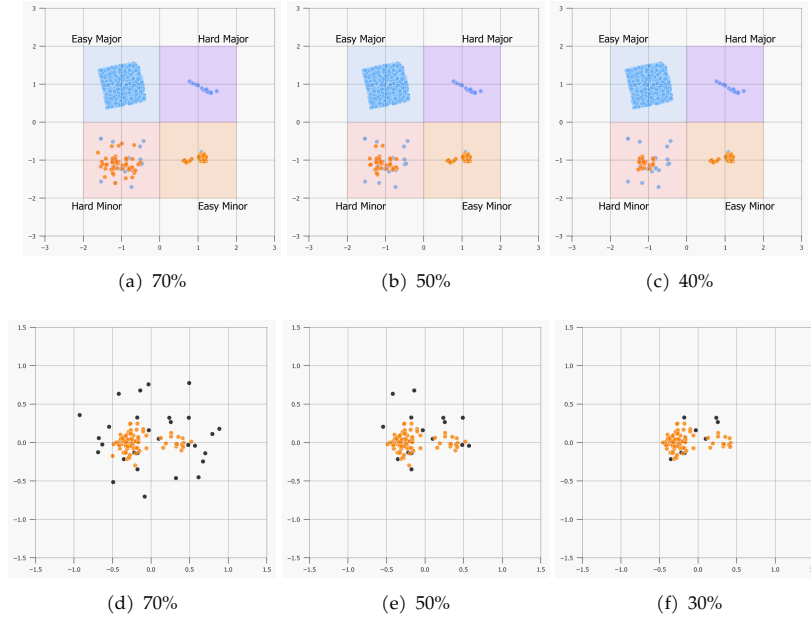


Fig. C3 Tuning  $\tau_2$  with visual representations.

## Appendix D Other evaluation metrics

This section presents the classification performances of benchmark methods using additional evaluation metrics, specifically the F1-score and geometric mean. Our proposed method consistently achieves higher performance in both of these metrics.

### F1-score

- $F1\text{-score} = 2 \times \frac{\text{Precision} \times \text{Recall}}{\text{Precision} + \text{Recall}}$

### Geometric mean (G-MEAN)

- $G\text{-MEAN} = \sqrt{\text{Sensitivity (Positive accuracy)} \times \text{Specificity (Negative accuracy)}}$

**Table 4** Classification performance (AUPRC) of different oversampling models using the random forest on the imbalanced datasets. The numbers within parentheses indicate their rankings, excluding BASE. The most favorable value is bolded.

Dataset	BASE	SMOTE	BSMOTE	SMOTE-ENN	KMSMOTE	DFBS	CVAE	DeepSMOTE	DDHS	SMOTE-CLS
ecoli	0.736 $\pm$ 0.064	0.674 $\pm$ 0.057	(7) 0.649 $\pm$ 0.106	(8) 0.720 $\pm$ 0.097	(4) 0.711 $\pm$ 0.061	(6) 0.639 $\pm$ 0.052	(9) 0.714 $\pm$ 0.080	(5) 0.736 $\pm$ 0.080	(2) <b>0.776<math>\pm</math>0.061</b>	(1) 0.722 $\pm$ 0.083
libras.move	0.531 $\pm$ 0.046	0.424 $\pm$ 0.133	(9) 0.437 $\pm$ 0.076	(7) 0.428 $\pm$ 0.130	(8) 0.460 $\pm$ 0.091	(6) 0.583 $\pm$ 0.059	(3) 0.597 $\pm$ 0.094	(2) <b>0.637<math>\pm</math>0.085</b>	(1) 0.543 $\pm$ 0.091	(5) 0.544 $\pm$ 0.102
spectrometer	0.731 $\pm$ 0.049	0.761 $\pm$ 0.049	(4) 0.741 $\pm$ 0.030	(6) 0.761 $\pm$ 0.034	(3) 0.756 $\pm$ 0.021	(5) 0.726 $\pm$ 0.073	(8) 0.737 $\pm$ 0.058	(7) <b>0.783<math>\pm</math>0.053</b>	(1) 0.556 $\pm$ 0.046	(9) 0.780 $\pm$ 0.053
oil	0.651 $\pm$ 0.076	0.563 $\pm$ 0.054	(8) 0.619 $\pm$ 0.080	(5) 0.548 $\pm$ 0.063	(9) 0.610 $\pm$ 0.081	(6) 0.683 $\pm$ 0.044	(2) 0.565 $\pm$ 0.125	(7) 0.633 $\pm$ 0.076	(4) <b>0.712<math>\pm</math>0.073</b>	(1) 0.662 $\pm$ 0.063
yeast	0.191 $\pm$ 0.056	0.340 $\pm$ 0.078	(4) 0.351 $\pm$ 0.069	(3) 0.330 $\pm$ 0.066	(5) <b>0.368<math>\pm</math>0.065</b>	(1) 0.172 $\pm$ 0.018	(8) 0.238 $\pm$ 0.043	(6) 0.180 $\pm$ 0.049	(7) 0.158 $\pm$ 0.031	(9) 0.357 $\pm$ 0.070
car.eval	0.904 $\pm$ 0.037	0.920 $\pm$ 0.034	(6) 0.920 $\pm$ 0.034	(5) 0.921 $\pm$ 0.027	(4) 0.930 $\pm$ 0.017	(2) 0.927 $\pm$ 0.026	(3) 0.905 $\pm$ 0.046	(8) 0.909 $\pm$ 0.054	(7) 0.891 $\pm$ 0.026	(9) <b>0.931<math>\pm</math>0.013</b>
us_crime	0.386 $\pm$ 0.044	0.413 $\pm$ 0.030	(5) <b>0.443<math>\pm</math>0.033</b>	(1) 0.395 $\pm$ 0.048	(8) 0.418 $\pm$ 0.018	(4) 0.428 $\pm$ 0.027	(2) 0.404 $\pm$ 0.022	(6) 0.399 $\pm$ 0.034	(7) 0.361 $\pm$ 0.032	(9) 0.425 $\pm$ 0.023
scene	0.264 $\pm$ 0.043	0.287 $\pm$ 0.029	(4) 0.295 $\pm$ 0.019	(3) 0.259 $\pm$ 0.022	(7) 0.296 $\pm$ 0.016	(2) 0.261 $\pm$ 0.017	(6) 0.233 $\pm$ 0.018	(8) 0.226 $\pm$ 0.024	(9) 0.266 $\pm$ 0.022	(5) <b>0.305<math>\pm</math>0.025</b>
abalone	0.284 $\pm$ 0.014	0.314 $\pm$ 0.014	(2) 0.312 $\pm$ 0.011	(4) 0.306 $\pm$ 0.008	(6) 0.235 $\pm$ 0.009	(9) 0.302 $\pm$ 0.014	(7) 0.313 $\pm$ 0.030	(3) 0.309 $\pm$ 0.019	(5) 0.265 $\pm$ 0.013	(8) <b>0.326<math>\pm</math>0.014</b>
optical.digits	0.914 $\pm$ 0.013	0.926 $\pm$ 0.012	(2) 0.876 $\pm$ 0.023	(7) 0.914 $\pm$ 0.018	(3) 0.905 $\pm$ 0.019	(4) 0.882 $\pm$ 0.013	(6) 0.870 $\pm$ 0.020	(8) 0.864 $\pm$ 0.020	(9) 0.888 $\pm$ 0.008	(5) <b>0.929<math>\pm</math>0.009</b>
satimage	0.711 $\pm$ 0.013	0.683 $\pm$ 0.019	(4) 0.577 $\pm$ 0.023	(7) 0.574 $\pm$ 0.036	(8) 0.532 $\pm$ 0.024	(9) 0.656 $\pm$ 0.014	(6) 0.723 $\pm$ 0.011	(2) <b>0.725<math>\pm</math>0.013</b>	(1) 0.679 $\pm$ 0.021	(5) 0.697 $\pm$ 0.009
isolet	0.796 $\pm$ 0.031	0.789 $\pm$ 0.027	(2) 0.697 $\pm$ 0.028	(9) 0.740 $\pm$ 0.038	(6) 0.763 $\pm$ 0.033	(5) 0.724 $\pm$ 0.025	(7) 0.768 $\pm$ 0.033	(4) 0.769 $\pm$ 0.026	(3) 0.698 $\pm$ 0.024	(8) <b>0.798<math>\pm</math>0.027</b>
Average rank	-	4.75	5.42	5.92	5.00	5.58	5.5	4.58	6.17	<b>2.08</b>



**Table 5** Classification performance (AUC) of different oversampling models using the random forest on the imbalanced datasets. The numbers within parentheses indicate their rankings, excluding BASE. The most favorable value is bolded.

Dataset	BASE	SMOTE	BSMOTE	SMOTE-ENN	KMSMOTE	DFBS	CVAE	DeepSMOTE	DDHS	SMOTE-CLS
ecoli	0.966 $\pm$ 0.012	0.961 $\pm$ 0.009	(7) 0.951 $\pm$ 0.012	(9) 0.966 $\pm$ 0.013	(5) 0.967 $\pm$ 0.008	(3) 0.953 $\pm$ 0.010	(8) 0.969 $\pm$ 0.009	(2) <b>0.970</b> $\pm$ 0.014	(1) 0.966 $\pm$ 0.013	(5) 0.966 $\pm$ 0.009
libras.move	0.830 $\pm$ 0.076	0.777 $\pm$ 0.079	(9) 0.793 $\pm$ 0.050	(8) 0.800 $\pm$ 0.079	(7) 0.827 $\pm$ 0.041	(5) 0.849 $\pm$ 0.091	(4) 0.867 $\pm$ 0.087	(2) <b>0.887</b> $\pm$ 0.064	(1) 0.850 $\pm$ 0.053	(3) 0.811 $\pm$ 0.079
spectrometer	0.858 $\pm$ 0.024	0.886 $\pm$ 0.030	(5) 0.864 $\pm$ 0.018	(8) 0.887 $\pm$ 0.026	(4) 0.867 $\pm$ 0.007	(7) 0.869 $\pm$ 0.019	(6) 0.908 $\pm$ 0.024	(2) 0.908 $\pm$ 0.041	(3) 0.845 $\pm$ 0.026	(9) <b>0.909</b> $\pm$ 0.037
oil	0.968 $\pm$ 0.019	0.972 $\pm$ 0.007	(4) 0.973 $\pm$ 0.015	(3) 0.972 $\pm$ 0.009	(5) 0.942 $\pm$ 0.039	(9) <b>0.978</b> $\pm$ 0.008	(1) 0.952 $\pm$ 0.048	(8) 0.969 $\pm$ 0.013	(6) 0.964 $\pm$ 0.037	(7) 0.976 $\pm$ 0.009
yeast	0.801 $\pm$ 0.055	0.933 $\pm$ 0.020	(2) 0.908 $\pm$ 0.019	(3) <b>0.941</b> $\pm$ 0.012	(1) 0.900 $\pm$ 0.049	(5) 0.812 $\pm$ 0.054	(7) 0.881 $\pm$ 0.021	(6) 0.809 $\pm$ 0.037	(8) 0.809 $\pm$ 0.049	(9) 0.900 $\pm$ 0.032
car_eval	0.994 $\pm$ 0.002	0.995 $\pm$ 0.002	(2) 0.995 $\pm$ 0.002	(2) <b>0.995</b> $\pm$ 0.001	(1) 0.994 $\pm$ 0.001	(4) 0.994 $\pm$ 0.002	(6) 0.992 $\pm$ 0.006	(8) 0.993 $\pm$ 0.004	(7) 0.990 $\pm$ 0.002	(9) 0.994 $\pm$ 0.001
us_crime	0.884 $\pm$ 0.016	0.894 $\pm$ 0.014	(6) <b>0.908</b> $\pm$ 0.010	(1) 0.904 $\pm$ 0.011	(2) 0.898 $\pm$ 0.012	(4) 0.900 $\pm$ 0.014	(3) 0.890 $\pm$ 0.014	(7) 0.883 $\pm$ 0.008	(8) 0.868 $\pm$ 0.014	(9) 0.896 $\pm$ 0.014
scene	0.728 $\pm$ 0.031	0.770 $\pm$ 0.021	(6) <b>0.780</b> $\pm$ 0.022	(1) 0.773 $\pm$ 0.014	(3) 0.775 $\pm$ 0.017	(2) 0.770 $\pm$ 0.014	(4) 0.703 $\pm$ 0.027	(8) 0.691 $\pm$ 0.024	(9) 0.715 $\pm$ 0.027	(7) 0.770 $\pm$ 0.014
abalone	0.836 $\pm$ 0.005	0.846 $\pm$ 0.005	(2) 0.846 $\pm$ 0.005	(2) 0.843 $\pm$ 0.006	(4) 0.813 $\pm$ 0.009	(9) 0.835 $\pm$ 0.005	(6) 0.838 $\pm$ 0.008	(7) 0.842 $\pm$ 0.006	(5) 0.826 $\pm$ 0.009	(8) <b>0.849</b> $\pm$ 0.009
optical.digits	0.982 $\pm$ 0.004	0.986 $\pm$ 0.003	(2) 0.978 $\pm$ 0.005	(5) 0.984 $\pm$ 0.004	(3) 0.981 $\pm$ 0.005	(4) 0.972 $\pm$ 0.004	(7) 0.971 $\pm$ 0.006	(8) 0.968 $\pm$ 0.006	(9) 0.977 $\pm$ 0.003	(6) <b>0.987</b> $\pm$ 0.002
satimage	0.934 $\pm$ 0.007	0.942 $\pm$ 0.005	(3) 0.930 $\pm$ 0.005	(8) 0.930 $\pm$ 0.005	(8) 0.931 $\pm$ 0.003	(7) 0.935 $\pm$ 0.004	(6) 0.941 $\pm$ 0.006	(4) <b>0.944</b> $\pm$ 0.004	(1) 0.937 $\pm$ 0.005	(5) 0.943 $\pm$ 0.004
isolet	0.973 $\pm$ 0.004	<b>0.979</b> $\pm$ 0.002	(1) 0.961 $\pm$ 0.005	(8) 0.976 $\pm$ 0.003	(4) 0.976 $\pm$ 0.002	(3) 0.970 $\pm$ 0.004	(6) 0.971 $\pm$ 0.006	(5) 0.969 $\pm$ 0.006	(7) 0.964 $\pm$ 0.004	(9) 0.977 $\pm$ 0.004
Average rank	-	4.08	4.83	3.92	5.17	5.33	5.58	5.42	7.17	<b>3.00</b>

**Table D1** Classification performance (F1-score) of different oversampling models using the random forest on the imbalanced datasets. The numbers within parentheses indicate their rankings, excluding BASE. The most favorable value is bolded.

Dataset	BASE	SMOTE	BSMOTE	SMOTEENN	KMSMOTE	DFBS	CVAE	DeepSMOTE	DDHS	SMOTE-CLS
ecoli	0.784 $\pm$ 0.049	0.793 $\pm$ 0.042	(3) 0.777 $\pm$ 0.023	(6) 0.774 $\pm$ 0.017	(5) <b>0.840</b> $\pm$ 0.042	(1) 0.778 $\pm$ 0.034	(4) 0.751 $\pm$ 0.067	(8) 0.744 $\pm$ 0.070	(9) 0.761 $\pm$ 0.046	(7) 0.820 $\pm$ 0.030
libras.move	0.733 $\pm$ 0.091	0.624 $\pm$ 0.076	(8) 0.636 $\pm$ 0.091	(7) 0.614 $\pm$ 0.091	(9) 0.659 $\pm$ 0.089	(5) 0.702 $\pm$ 0.091	(2) 0.674 $\pm$ 0.121	(4) 0.675 $\pm$ 0.109	(3) <b>0.717</b> $\pm$ 0.081	(1) 0.640 $\pm$ 0.123
spectrometer	0.816 $\pm$ 0.055	0.819 $\pm$ 0.046	(6) 0.822 $\pm$ 0.035	(4) 0.819 $\pm$ 0.024	(5) <b>0.836</b> $\pm$ 0.030	(1) 0.748 $\pm$ 0.050	(8) 0.767 $\pm$ 0.066	(7) 0.833 $\pm$ 0.057	(3) 0.721 $\pm$ 0.046	(9) 0.833 $\pm$ 0.045
oil	0.704 $\pm$ 0.065	0.775 $\pm$ 0.037	(3) 0.764 $\pm$ 0.077	(4) <b>0.784</b> $\pm$ 0.054	(1) 0.652 $\pm$ 0.056	(9) 0.752 $\pm$ 0.045	(6) 0.669 $\pm$ 0.044	(8) 0.687 $\pm$ 0.056	(7) 0.756 $\pm$ 0.082	(5) 0.776 $\pm$ 0.032
yeast	0.507 $\pm$ 0.026	0.668 $\pm$ 0.047	(4) <b>0.706</b> $\pm$ 0.045	(1) 0.688 $\pm$ 0.021	(3) 0.697 $\pm$ 0.035	(2) 0.528 $\pm$ 0.036	(6) 0.514 $\pm$ 0.028	(8) 0.520 $\pm$ 0.039	(7) 0.495 $\pm$ 0.015	(9) 0.665 $\pm$ 0.049
car.eval	0.895 $\pm$ 0.019	0.934 $\pm$ 0.013	(3) <b>0.941</b> $\pm$ 0.009	(1) 0.940 $\pm$ 0.018	(2) 0.929 $\pm$ 0.019	(4) 0.901 $\pm$ 0.021	(6) 0.875 $\pm$ 0.036	(9) 0.886 $\pm$ 0.026	(8) 0.893 $\pm$ 0.016	(7) 0.927 $\pm$ 0.018
us-crime	0.615 $\pm$ 0.028	0.676 $\pm$ 0.026	(4) 0.667 $\pm$ 0.025	(5) 0.683 $\pm$ 0.013	(2) <b>0.686</b> $\pm$ 0.031	(1) 0.647 $\pm$ 0.020	(6) 0.619 $\pm$ 0.019	(8) 0.618 $\pm$ 0.038	(9) 0.645 $\pm$ 0.017	(7) 0.677 $\pm$ 0.033
scene	0.546 $\pm$ 0.017	0.626 $\pm$ 0.024	(2) 0.620 $\pm$ 0.021	(3) 0.558 $\pm$ 0.014	(6) 0.608 $\pm$ 0.021	(4) 0.546 $\pm$ 0.011	(7) 0.536 $\pm$ 0.001	(9) 0.539 $\pm$ 0.008	(8) 0.561 $\pm$ 0.019	(5) <b>0.633</b> $\pm$ 0.019
abalone	0.482 $\pm$ 0.011	0.654 $\pm$ 0.011	(5) 0.659 $\pm$ 0.010	(4) 0.587 $\pm$ 0.005	(6) 0.565 $\pm$ 0.012	(7) 0.680 $\pm$ 0.008	(2) 0.506 $\pm$ 0.015	(8) 0.499 $\pm$ 0.012	(9) <b>0.682</b> $\pm$ 0.007	(1) 0.662 $\pm$ 0.008
optical.digits	0.865 $\pm$ 0.014	0.911 $\pm$ 0.013	(2) 0.870 $\pm$ 0.014	(6) 0.893 $\pm$ 0.019	(4) 0.897 $\pm$ 0.011	(3) 0.849 $\pm$ 0.010	(7) 0.765 $\pm$ 0.039	(8) 0.669 $\pm$ 0.055	(9) 0.874 $\pm$ 0.011	(5) <b>0.915</b> $\pm$ 0.011
satimage	0.796 $\pm$ 0.010	0.787 $\pm$ 0.008	(6) 0.744 $\pm$ 0.007	(8) 0.737 $\pm$ 0.008	(9) 0.765 $\pm$ 0.014	(7) 0.792 $\pm$ 0.009	(4) 0.791 $\pm$ 0.012	(5) 0.801 $\pm$ 0.010	(2) <b>0.802</b> $\pm$ 0.016	(1) 0.795 $\pm$ 0.010
isolet	0.693 $\pm$ 0.023	0.817 $\pm$ 0.007	(3) 0.799 $\pm$ 0.015	(6) 0.781 $\pm$ 0.015	(7) 0.827 $\pm$ 0.012	(2) 0.800 $\pm$ 0.012	(5) 0.567 $\pm$ 0.026	(8) 0.539 $\pm$ 0.041	(9) 0.815 $\pm$ 0.013	(4) <b>0.831</b> $\pm$ 0.010
Average rank	-	4.08	4.58	4.92	3.83	5.25	7.5	6.92	5.08	<b>2.83</b>

**Table D2** Classification performance (G-MEAN) of different oversampling models using the random forest on the imbalanced datasets. The numbers within parentheses indicate their rankings, excluding BASE. The most favorable value is bolded.

Dataset	BASE	SMOTE	BSMOTE	SMOTEENN	KMSMOTE	DFBS	CVAE	DeepSMOTE	DDHS	SMOTE-CLS
ecoli	0.753 $\pm$ 0.063	0.904 $\pm$ 0.040	(4) 0.887 $\pm$ 0.041	(5) <b>0.919</b> $\pm$ 0.029	(1) 0.905 $\pm$ 0.060	(3) 0.805 $\pm$ 0.035	(6) 0.717 $\pm$ 0.062	(8) 0.705 $\pm$ 0.071	(9) 0.740 $\pm$ 0.047	(7) 0.915 $\pm$ 0.036
libras.move	0.670 $\pm$ 0.064	0.596 $\pm$ 0.059	(9) 0.613 $\pm$ 0.071	(6) 0.602 $\pm$ 0.076	(8) 0.616 $\pm$ 0.062	(5) 0.649 $\pm$ 0.066	(2) 0.629 $\pm$ 0.090	(4) 0.629 $\pm$ 0.077	(3) <b>0.659</b> $\pm$ 0.068	(1) 0.607 $\pm$ 0.084
spectrometer	0.749 $\pm$ 0.057	0.755 $\pm$ 0.051	(6) 0.755 $\pm$ 0.044	(5) 0.759 $\pm$ 0.025	(4) 0.767 $\pm$ 0.033	(2) 0.687 $\pm$ 0.045	(8) 0.705 $\pm$ 0.065	(7) 0.767 $\pm$ 0.060	(3) 0.684 $\pm$ 0.044	(9) <b>0.780</b> $\pm$ 0.057
oil	0.648 $\pm$ 0.050	0.772 $\pm$ 0.042	(2) 0.760 $\pm$ 0.084	(4) <b>0.818</b> $\pm$ 0.075	(1) 0.610 $\pm$ 0.046	(9) 0.708 $\pm$ 0.050	(5) 0.622 $\pm$ 0.039	(8) 0.635 $\pm$ 0.046	(7) 0.704 $\pm$ 0.074	(6) 0.772 $\pm$ 0.050
yeast	0.508 $\pm$ 0.015	0.698 $\pm$ 0.064	(3) 0.716 $\pm$ 0.055	(2) <b>0.809</b> $\pm$ 0.032	(1) 0.673 $\pm$ 0.034	(4) 0.522 $\pm$ 0.025	(6) 0.512 $\pm$ 0.016	(8) 0.515 $\pm$ 0.023	(7) 0.501 $\pm$ 0.009	(9) 0.662 $\pm$ 0.048
car.eval	0.873 $\pm$ 0.026	0.954 $\pm$ 0.021	(4) 0.970 $\pm$ 0.015	(3) <b>0.981</b> $\pm$ 0.015	(1) 0.937 $\pm$ 0.028	(6) 0.940 $\pm$ 0.024	(5) 0.835 $\pm$ 0.046	(9) 0.840 $\pm$ 0.044	(8) 0.971 $\pm$ 0.010	(2) 0.926 $\pm$ 0.034
us_crime	0.589 $\pm$ 0.022	0.650 $\pm$ 0.027	(3) 0.638 $\pm$ 0.024	(5) <b>0.822</b> $\pm$ 0.026	(1) 0.695 $\pm$ 0.036	(2) 0.616 $\pm$ 0.017	(6) 0.592 $\pm$ 0.015	(8) 0.590 $\pm$ 0.029	(9) 0.612 $\pm$ 0.015	(7) 0.646 $\pm$ 0.036
scene	0.534 $\pm$ 0.010	0.611 $\pm$ 0.023	(3) 0.602 $\pm$ 0.017	(4) <b>0.664</b> $\pm$ 0.025	(1) 0.581 $\pm$ 0.017	(5) 0.535 $\pm$ 0.007	(7) 0.528 $\pm$ 0.000	(9) 0.530 $\pm$ 0.004	(8) 0.543 $\pm$ 0.011	(6) 0.616 $\pm$ 0.019
abalone	0.847 $\pm$ 0.005	0.853 $\pm$ 0.007	(3) 0.852 $\pm$ 0.006	(5) 0.778 $\pm$ 0.005	(8) 0.564 $\pm$ 0.011	(9) <b>0.857</b> $\pm$ 0.006	(1) 0.849 $\pm$ 0.008	(7) 0.852 $\pm$ 0.006	(5) 0.853 $\pm$ 0.010	(4) 0.853 $\pm$ 0.006
optical.digits	0.807 $\pm$ 0.017	0.925 $\pm$ 0.011	(2) 0.903 $\pm$ 0.008	(7) 0.917 $\pm$ 0.014	(4) 0.910 $\pm$ 0.008	(6) 0.916 $\pm$ 0.008	(5) 0.700 $\pm$ 0.037	(8) 0.619 $\pm$ 0.038	(9) 0.917 $\pm$ 0.008	(3) <b>0.927</b> $\pm$ 0.012
satimage	0.756 $\pm$ 0.012	0.782 $\pm$ 0.014	(3) 0.801 $\pm$ 0.011	(2) <b>0.838</b> $\pm$ 0.008	(1) 0.779 $\pm$ 0.018	(6) 0.779 $\pm$ 0.009	(5) 0.749 $\pm$ 0.011	(9) 0.755 $\pm$ 0.011	(8) 0.766 $\pm$ 0.008	(7) 0.780 $\pm$ 0.011
isolet	0.634 $\pm$ 0.019	0.860 $\pm$ 0.009	(3) 0.803 $\pm$ 0.018	(6) <b>0.932</b> $\pm$ 0.010	(1) 0.929 $\pm$ 0.008	(2) 0.846 $\pm$ 0.010	(4) 0.538 $\pm$ 0.016	(8) 0.501 $\pm$ 0.004	(9) 0.795 $\pm$ 0.010	(7) 0.836 $\pm$ 0.016
Average rank	-	3.75	4.50	<b>2.67</b>	4.92	5.00	7.75	7.08	5.67	3.58